

1 **Investigation of short-term effective radiative forcing of fire**  
2 **aerosols over North America using nudged hindcast ensembles**

3 Yawen Liu<sup>1,2</sup>, Kai Zhang<sup>2</sup>, Yun Qian<sup>2</sup>, Yuhang Wang<sup>3</sup>, Yufei Zou<sup>3</sup>, Yongjia Song<sup>3</sup>, Hui Wan<sup>2</sup>,  
4 Xiaohong Liu<sup>4</sup>, and Xiu-Qun Yang<sup>1</sup>

5 <sup>1</sup>School of Atmospheric Sciences, Nanjing University, Nanjing, China

6 <sup>2</sup>Pacific Northwest National Laboratory, Richland, Washington, USA

7 <sup>3</sup>School of Earth and Atmospheric Sciences, Georgia Institute of Technology, Atlanta, Georgia, USA

8 <sup>4</sup>Department of Atmospheric Science, University of Wyoming, Laramie, Wyoming, USA

9

10

11 Corresponding to: Yun Qian [Yun.Qian@pnnl.gov]

12

13

14

15

16

17

18

## 19 **Abstract**

20 Aerosols from fire emissions can potentially have large impact on clouds and radiation. However, fire aerosol  
21 sources are often intermittent and their effect on weather and climate is difficult to quantify. Here we investigated  
22 the short-term effective radiative forcing of fire aerosols using the global aerosol-climate model Community  
23 Atmosphere Model Version 5 (CAM5). Different from previous studies, we used nudged hindcast ensembles to  
24 quantify the forcing uncertainty due to the chaotic response to small perturbations in the atmosphere state. Daily  
25 mean emissions from three fire inventories were used to consider the uncertainty in emission strength and injection  
26 heights. The simulated aerosol optical depth (AOD) and mass concentrations were evaluated against in-situ  
27 measurements and re-analysis data. Overall, the results show the model has reasonably good predicting skills. Short  
28 (10-day) nudged ensemble simulations were then performed with and without fire emissions to estimate the effective  
29 radiative forcing. Results show fire aerosols have large effects on both liquid and ice clouds over the two selected  
30 regions in April 2009. Ensemble mean results show strong negative shortwave cloud radiative effect (SCRE) over  
31 almost the entire Southern Mexico, with a 10-day regional mean value of  $-3.02\text{W m}^{-2}$ . Over the Central U.S, the  
32 SCRE is positive in the north but negative in the south and the regional mean SCRE is small ( $-0.56\text{W m}^{-2}$ ). For the  
33 10-day average, we found a large ensemble spread of regional mean shortwave cloud radiative effect over Southern  
34 Mexico (15.6% of the corresponding ensemble mean) and the Central U.S. (64.3%), despite that the regional mean  
35 AOD time series are almost indistinguishable during the 10-day period. Moreover, the ensemble spread is much  
36 larger when using daily averages instead of 10-day averages. This demonstrates the importance of using a large  
37 ensemble of simulations to estimate the short-term aerosol effective radiative forcing.

## 38 **1. Introduction**

39 Natural and human-induced fires play an important role in the Earth system. Aerosol and gas emissions from  
40 biomass burning can change the atmospheric composition and potentially affect the weather and climate. Over 30%  
41 of the global total emission of black carbon (BC) comes from open burning of forests, grasslands and agricultural  
42 residues (Bond et al. 2013). For organic aerosols, substantial increases of concentrations dominated by organic  
43 carbon enhancements are observed in regions with biomass burning events (Zeng et al. 2011; Lin et al. 2013; Brito  
44 et al. 2014; Reddington et al. 2014). As a result, biomass burning emissions have a large impact on the global and  
45 regional mean aerosol optical depth (Jacobson, 2014).

46 Through interactions with radiation and cloud, fire aerosols can significantly affect the long-term Earth's energy  
47 budget. Previous studies have investigated the global and regional radiative forcing of fire aerosols using long  
48 climatological simulations or satellite retrievals. For example, Ward et al. (2012) investigated the radiative forcing  
49 of global fires in pre-industrial, present day, and future periods. For the present-day condition, they estimated a  
50 direct aerosol effect (or radiative forcing through aerosol–radiation interactions as defined in IPCC AR5, RFari; see  
51 section 2.4) of  $+0.1\text{W m}^{-2}$  and an indirect effect (radiative forcing through aerosol–cloud interactions, RFaci) of -  
52  $1.0\text{W m}^{-2}$ . Using a newer model, Jiang et al. (2016) found similar RFari but slightly smaller RFaci ( $-0.70\text{W m}^{-2}$ ).  
53 Sena et al. (2013) assessed the direct impact of biomass burning aerosols over the Amazon basin using satellite data.  
54 Over the 10-year study period, the estimated radiative forcing is about  $-5.6\text{W m}^{-2}$ .

55 On short timescales, fire aerosols have even larger radiative impacts. Observed maximum daily direct aerosol  
56 radiative effects can reach  $-20\text{ W m}^{-2}$  at TOA locally in Amazonia during biomass burning seasons (Sena et al.,  
57 2013). Very large direct effects of fire aerosols were observed during extreme fire events over Central Russia  
58 (Tarasova et al. 2004; Chubarova et al. 2008; Chubarova et al. 2012). Instantaneous direct radiative effects of  
59 emitted aerosols reached  $-167\text{ W m}^{-2}$  and monthly mean direct radiative effects reached about  $-65\text{ W m}^{-2}$  in the  
60 2010 Russia wildfires (Chubarova et al. 2012). Kolusu et al. (2015) investigated direct radiative effect of biomass  
61 burning aerosols over tropical Southern America. By quantifying results from the first and second day of 2-day  
62 single-member forecasts in September 2012, they found the modeled biomass burning aerosols reduced all-sky net  
63 radiation by  $8\text{ W m}^{-2}$  at TOA and  $15\text{ W m}^{-2}$  at surface. Fire aerosol indirect effect may also significantly affect the  
64 cloud formation and radiative balance on short time scales. Using satellite data and a radiative transfer model,  
65 Kaufman et al. (2005) found an indirect radiative effect of  $-9.5\text{ W m}^{-2}$  due to smoke aerosol-induced cloud changes  
66 over Southeast Atlantic for the 3 months studied. Smoke-derived cloud albedo effect on local shortwave radiative  
67 forcing is estimated to be between  $-2$  and  $-4\text{ W m}^{-2}$  in a day case study of aircraft-measured indirect cloud effects  
68 (Zamora et al., 2016)..

69 Previous modeling studies on the short-term fire aerosol effects mainly focused on aerosol direct effects (e.g.,  
70 Keil and Haywood, 2003; Chen et al., 2014; Kolusu et al., 2015), and only a couple of studies investigated the  
71 indirect effects of fire aerosols (Lu et al. 2013). In addition, to estimate the aerosol indirect effect, long simulations  
72 (multi-years,  $>5$  years preferred) are often needed to remove the noise, because aerosol life cycle and cloud  
73 properties are affected by strong natural variability on different timescales (Bony et al. 2006; Kooperman et al.  
74 2012). To solve the problem, alternative methods have been proposed to help extract signals with shorter  
75 simulations. For example, nudging (also called Newton relaxation method) can help reduce uncertainties associated  
76 with natural variability by constraining certain meteorological fields towards prescribed conditions. A robust  
77 estimate of global anthropogenic aerosol indirect effects can be obtained on substantially shorter timescales (1-2  
78 years) by implementing nudging to constrain simulations with pre-industrial and present-day aerosol emissions  
79 toward identical circulation and meteorology (Kooperman et al. 2012). When nudged towards re-analysis data,  
80 Zhang et al. (2014) found constraining only the horizontal winds is a preferred strategy to estimate the aerosol  
81 indirect effect since it provides well-constrained meteorology without strongly perturbing the model's mean climate  
82 state. Another example is the use of representative ensembles of short simulations to replace a typical long  
83 integration. Wan et al. (2014) explored the feasibility of this method and showed that 3-day ensembles of 20 to 50  
84 members are able to reveal the main signals revealed by traditional 5-year simulations.

85 In this study, we performed month-long and 10-day nudged CAM5 simulations to investigate the effects of fire  
86 aerosols on radiation and cloud processes on short time scales (less than two weeks). Horizontal winds were nudged  
87 towards 6-hourly reanalysis to constrain the large-scale circulation and to allow for more accurate model evaluations  
88 against observations. We also used daily mean emissions from three fire inventories to consider the uncertainty in  
89 emission strength and injection heights. Even for short simulations, small perturbations of meteorological states  
90 might have large impact on the local aerosol and cloud properties, thus bring uncertainty to the aerosol forcing

91 estimate. Therefore, in our simulations, we also employed very weak temperature nudging (~10days) in combination  
92 with ensembles to quantify the uncertainty. More details of the nudging setup are described in section2.3.

93 The rest of the paper is organized as follows. Sect. 2 describes the model and data used in this study. It also  
94 introduces how the ensembles are generated in the short nudged simulations and explains how the fire aerosol  
95 forcing is estimated. Results and discussions are presented in Sect. 3 and conclusions are summarized in Sect. 4

## 96 **2. Model, Method and Data**

### 97 **2.1 Model description**

98 In this study, we used the Community Atmosphere Model (CAM) version 5.3 with the finite volume dynamical core  
99 at  $1.9^\circ$  (latitude)  $\times$   $2.5^\circ$  (longitude) horizontal resolution with 30 vertical layers. The aerosol life cycle is represented  
100 using the modal aerosol module MAM3 (Liu et al., 2012). CAM5 links the simulated aerosol fields with cloud and  
101 radiation through interactions of the aerosol module with the cloud microphysics and radiative transfer  
102 parameterizations. The two-moment bulk cloud microphysics scheme from Morrison and Gettelman (2008) is used  
103 to track mass mixing ratios and number concentrations of cloud droplets and ice crystals in stratiform clouds.  
104 Representation of shallow convection is based on the work of Park and Bretherton (2009). The deep convection  
105 parameterization was developed by Zhang and McFarlane (1995) and later revised by Richter and Rasch (2008) and  
106 Neale et al. (2008). Longwave and shortwave radiative transfer are calculated with the Rapid Radiative Transfer  
107 Model for GCMs (RRTMG, Malwer et al. 1997; Iacono et al. 2008).

### 108 **2.2 Fire Emission Inventories**

109 Three fire emission inventories were used in this study. Two of them are widely used bottom-up inventories—  
110 Global Fire Emissions Database version 3.1 (GFED v3.1, van der Werf et al., 2010; [https://daac.ornl.gov/cgi-  
111 bin/dsviewer.pl?ds\\_id=1191](https://daac.ornl.gov/cgi-bin/dsviewer.pl?ds_id=1191)) and GFED v4.1s (Giglio et al. 2013; Randerson et al. 2012;  
112 [https://daac.ornl.gov/VEGETATION/guides/fire\\_emissions\\_v4.html](https://daac.ornl.gov/VEGETATION/guides/fire_emissions_v4.html)). Another one is a top-down emission  
113 inventory—Quick Fire Emissions Dataset version 2.4 (QFED v2.4). GFED v3.1 and GFED v4.1s provide global  
114 monthly emissions at  $0.25 \times 0.25$  degree spatial resolution from 1997 through the present. Daily emission data can be  
115 obtained by disaggregating monthly emissions based on daily temporal variability in fire emissions derived from  
116 MODIS measurements of active fires (Mu et al. 2011). The daily emission data is obtained using daily scalars  
117 (<http://www.globalfiredata.org/data.html>) to distribute monthly emissions over the days and is only available from  
118 2003 onwards. The more recent version GFED v4.1s improves by including small fires based on active fire  
119 detections outside the burned area maps (Randerson et al., 2012). QFED v2.4 estimates global fire emissions using  
120 the Moderate Resolution Imaging Spectroradiometer (MODIS) measurements of fire radiative power and generates  
121 daily products at  $0.1 \times 0.1$  degree resolution.

122 To drive CAM5 simulations, fire emission data were regridded to the model resolution and distributed vertically.  
123 For the GFED v3.1 and QFED v2.4 emission data we adopted the same injection heights (from surface to 6 km) as

124 used in the standard CAM5 model. While for GFEDv4.1s, in this study the injection heights were estimated using a  
125 fire plume model and scaled to the 6-hourly interval.

126 The fire emission inventories were first analyzed to select appropriate time periods and regions for our study  
127 before being used to drive model simulations. Fig.1 shows the multi-year mean biomass burning emissions from  
128 GFED v4.1 over North America. The emission manifests significant seasonality with large dry matter consumption  
129 during March to April and June to September. The summer and autumn burning covers Pacific Northwest and part  
130 of Canada and is mainly associated with forest fires, while the spring burning occurs in more densely populated  
131 regions like Mexico and central and eastern United States with a large contribution of agricultural fires in croplands  
132 (Korontzi et al., 2006; Magi et al., 2012). Similar features are also captured in GFED v3.1 and QFED v2.4 with  
133 differences in the magnitude. We chose to analyze the simulated fire aerosol effect in April, the peak month of  
134 spring burning, when there are extreme fire activities over Mexico (10 N to 25N, 100W to 80W) and occasionally  
135 large fires in the Central U.S. (35 N to 45N, 100W to 85W). For the U.S., extended fire period is rare, making it  
136 necessary to perform short-term evaluation. Fire aerosols formed from these two regions are often transported to the  
137 Eastern and Southeastern U.S., where they mix with aerosols from anthropogenic sources and potentially have  
138 significant impact on clouds and radiation over these areas. Time series of regional mean fire emissions in April  
139 during 2003-2014 shows that relatively large fires occur in both regions in 2009 (Fig.S1). Values of fire emissions in  
140 2009 are larger than the multi-year April mean by a factor of 1.9 in the Central U.S. and 1.5 in Southern Mexico.  
141 Thus, in the following model simulations, we focused on analyzing the aerosol properties and radiative effects over  
142 the two selected regions (denoted by the red boxes in Fig.1) in April, 2009.

143 Fire emitted BC from different emission inventories in April, 2009 is shown in Fig.2. Although GFED v4.1s  
144 includes the contributions of small fires (Randerson et al., 2012), the emitted BC in GFED v4.1 shows no substantial  
145 increase compared to GFED v3.1 during the selected period. Only an increase by 1.75 is seen over Southern Mexico.  
146 In the Central U.S., the BC emission is even slightly weaker in GFED v4.1. QFED v2.4 shows a much larger BC  
147 emission than the GFED inventories. Monthly mean values of emitted BC in QFED v2.4 are larger than those in  
148 GFED v4.1s by a factor of 11.4 in the Central U.S. and a factor of 3.3 in Southern Mexico.

### 149 **2.3 Simulations**

150 Two groups of simulations were conducted (Table1) using the same greenhouse gas concentrations, sea surface  
151 conditions and anthropogenic emissions of aerosols and precursors. Each group includes four simulations,  
152 performed either without fire emission or with daily fire emissions from one of the three fire emission inventories  
153 introduced in section 2.2. The emitted species include BC, OC, and SO<sub>2</sub>. Horizontal winds were nudged to 6-hourly  
154 ERA-Interim reanalysis (Dee et al., 2011) as described in Zhang et al. (2014) in both groups.

155 Simulations in Group A are month-long single-member nudged simulations. These simulations were performed  
156 to provide longer time series for model evaluation and generate initial condition files for simulations in Group B.  
157 They started from January 1, 2009 and were integrated for four months with 3-month spin-up. Initial condition files  
158 were generated on April 1 at 00 UTC for simulations in group B.

159 Simulations in group B are 10-day ensemble simulations. Unlike the traditional way of perturbing initial  
160 conditions, in this study we constructed the ensembles by implementing a very weak temperature nudging and  
161 perturbing the nudging time scale. This is because under the influence of horizontal-wind nudging, ensemble  
162 differences generated by perturbing initial conditions would fade away during the integration. In contrast, our  
163 method can consider the influence of small temperature perturbations during the entire simulation period, as nudging  
164 is applied at every time step. On the other hand, the large-scale circulation patterns simulated in the different  
165 ensemble members are very similar (not shown), so the noises caused by the chaotic system can be constrained and  
166 the effective fire aerosol forcing signal can be easily identified.

167 Each ensemble in group B includes 10 members. The only difference between the members is the relaxation time  
168 scale of temperature, which varies from 10 to 11 days at an interval of 0.1 day. All simulations started on April 1,  
169 2009 and were integrated for 10 days. For each simulation (e.g. E\_QF), the initial condition was generated by  
170 combining the meteorological fields from initial condition outputs in the S\_NF simulation with aerosol and  
171 precursor concentrations from initial condition outputs in the single-member simulation forced by the corresponding  
172 fire emission (S\_QF).

#### 173 **2.4 Calculation of fire aerosol RF**

174 The IPCC AR5 report provides a more useful characterization of aerosol forcing by allowing for rapid  
175 tropospheric adjustments (Boucher et al., 2013) compared to the original definition of aerosol forcing. It quantifies  
176 aerosol radiative effects in terms of Effective Radiative Forcing from aerosol-radiation interactions (ERFari) and  
177 Effective Radiative Forcing from aerosol-cloud interactions (ERFaci). ERFari refers to the combined effect of  
178 instantaneous radiative forcing from direct scattering and absorption of sunlight (aerosol direct effect) and related  
179 subsequent rapid adjustments of atmospheric state variables and cloudiness (aerosol semi-direct effect). ERFaci  
180 refers to the indirect forcing resulting from aerosol induced changes in cloud albedo (first albedo effect) and  
181 subsequent changes in cloud lifetime as rapid adjustments (second aerosol indirect effect) via microphysical  
182 interactions.

183 To allow for a straightforward comparison with previous studies in the literature, we followed the IPCC concept  
184 of including rapid adjustments (effective aerosol radiative forcing), but continued to decompose the aerosol effect in  
185 the conventional terms as aerosol direct radiative effect (DRE), aerosol cloud radiative effect (CRE) and surface  
186 albedo effect. Note that as nudging timescale determines the degree to which model physics are constrained  
187 (Kooperman et al., 2012), the use of a 6-hour relaxation time scale for horizontal wind nudging means only very fast  
188 adjustments are considered in the simulations.

189 Similar to Jiang et al. (2016), our calculations are based on the work of Ghan et al. (2012) and Ghan (2013). Fire  
190 aerosol DRE, CRE and surface albedo effect are defined as fire induced changes in aerosol forcing, cloud forcing,  
191 and surface albedo forcing respectively, and are calculated as the difference of each item between simulations with  
192 and without fire emissions (denoted by  $\Delta$ ). In each simulation, aerosol forcing was defined as the difference between  
193 all-sky and clean-sky TOA radiative fluxes ( $F - F_{\text{clean}}$ ). Cloud forcing was defined as the difference between all-sky  
194 and clear sky TOA radiative fluxes under clean-sky conditions ( $F_{\text{clean}} - F_{\text{clean,clear}}$ ). The rest were related to

195 surface albedo forcing ( $F_{\text{clean,clear}}$ ). Thus fire aerosol DRE, CRE, and surface albedo effect were expressed  
196 as  $\Delta(F - F_{\text{clean}})$ ,  $\Delta(F_{\text{clean}} - F_{\text{clean,clear}})$ , and  $\Delta F_{\text{clean,clear}}$ , respectively. More details about the method can be found  
197 in section 2 of Ghan (2013). CRE includes contributions of both aerosol indirect effect and aerosol semi-direct effect  
198 but was analyzed as a single term (i.e., the sum).

## 199 2.5 Observational Data

200 In this study, we used two sets of AOD reanalysis and the AERONET data (Holben et al. 1998) to evaluate the  
201 modeled AOD. The two AOD reanalysis datasets are the Naval Research Laboratory (NRL) reanalysis (Rubin et al.  
202 2015) and the Monitoring Atmospheric Composition and Climate (MACC) reanalysis (Eskes et al. 2015). Both are  
203 generated by assimilating AOD retrievals from MODIS (Zhang et al., 2008; Benedetti et al., 2009) with forecast  
204 fields. The NRL reanalysis provides 6-hourly AOD at 1°horizontal resolution. The MACC dataset provides 3-  
205 hourly AOD at 1.125°horizontal resolution. Daily averages in April, 2009 were used for model evaluation in this  
206 study. AERONET retrievals of AOD from April 1 to April 30 in 2009 were used for model evaluation. Two sites are  
207 available in the selected regions: Cart\_Site (36°N, 97°W) and Mexico\_City (19°N, 99°W). LEV 2.0 cloud-screened  
208 all points AOD at 500 nm and 675 nm was used to generate hourly AOD at 550nm, which are the processed data  
209 based on a cloud-screening algorithm (Smirnov et al. 2000).

210 In addition, the simulated BC and primary organic matter (POM) concentrations were compared with  
211 observations from the Interagency Monitoring of Protected Visual Environments (IMPROVE) (Malm et al. 2004).  
212 IMPROVE aerosol data are only available over the Central U.S. A total of fifteen sites were selected and marked in  
213 Fig 2, which include the sites west of 94°W near the source region (asterisks) and sites east of 94°W in the  
214 downwind region (dots). Observed organic carbon concentrations were multiplied by 1.4 for comparison with  
215 simulated POM. Detailed descriptions about the data and sites are available at  
216 <http://vista.cira.colostate.edu/improve/>. The IMPROVE network collect 24-hour aerosol data on every third day.  
217 Daily averages during April, 2009 are compared on IMPROVE observation days only.

## 218 3. Results

219 In this part, the model performance is first evaluated based on the simulations in group A. Next, we present the  
220 simulated short-term effective fire aerosol forcing on 10-day and daily timescales based on the results from group B  
221 simulations. We will demonstrate the importance of using ensemble simulations in estimating the short-term aerosol  
222 effective forcing and give a quantitative estimate of how many ensemble members are needed for the case selected  
223 in this study.

### 224 3.1 Model Evaluation

225 Model simulated AOD are evaluated against the NRL and MACC reanalysis data (Fig. 3). The simulated temporal  
226 variation of regional mean AOD over the central U.S. is consistent with that in the reanalysis, but the magnitudes of  
227 simulated AOD are lower (Fig. 3). A better agreement is found between the model and the NRL data, despite the

228 horizontal winds in the simulation are nudged towards a reanalysis that is very similar to the data used to derive  
229 MACC. Temporal correlation coefficients (TCC) between the modeled AOD and the NRL reanalysis are 0.87 and  
230 0.82 for S\_QF and S\_GF4 simulations, respectively, but are lower (0.67 and 0.78) between the modeled AOD and  
231 the MACC reanalysis data. The corresponding root mean square errors rise from 0.13 (S\_QF) and 0.1 (S\_GF4) to  
232 0.23 and 0.21. Generally, AOD is underestimated by a factor of 2-4 in all simulations compared to the reanalysis,  
233 especially in simulations with GFED emissions. Previous studies have found the underestimation of AOD in  
234 simulations with GFED emissions and suggested the need to scale up GFED emissions by a factor of 1-3 to match  
235 the observed AOD (Tosca et al., 2013). This is consistent with the large negative bias in the simulation S\_GF3 and  
236 S\_GF4. However, a much larger scale factor might be needed in this case. Simulated AOD in these two simulations  
237 are almost indistinguishable due to the small difference in the total fire emission in the region.

238 Over Mexico, different simulations produce similar temporal variations in AOD, but the magnitude is smaller in  
239 the GFED simulations. Fire aerosol-induced AOD increase accounts for 8.1% (S\_GF3), 11.2% (S\_GF4) and 48.8%  
240 (S\_QF) of the background AOD (Table S2). Large discrepancies are found between model results and reanalysis  
241 data during Apr. 17-20. An increase of AOD is captured by both reanalysis datasets, while model results display a  
242 decrease of AOD compared to earlier days in the simulation period. Note that the two sets of reanalysis data also  
243 have some differences occasionally. For example, during Apr. 10-12, NRL data displays an increase of AOD, while  
244 MACC data show the opposite. These discrepancies may partly result from the large internal variability in this  
245 tropical region, where the simulated atmosphere state and its influence on aerosol transport are more likely to  
246 disagree between the model and the reanalysis. Generally speaking, the model forced with different fire emissions is  
247 capable of capturing daily variation of AOD in both regions, especially during Apr. 1-10. This period was selected  
248 for further investigation of the short-term fire aerosol effect.

249 Model simulated AOD are also evaluated against AERONET retrievals (Fig. 4). At Cart Site (36°N, 97°W), with  
250 the QFED emission (S\_QF) the model performs well in simulating both the temporal variation (TCC=0.62) and  
251 magnitude of AOD. Simulations with GFED emissions also reproduce the temporal evolution well (TCC = 0.58 for  
252 S\_GF3 and 0.55 for S\_GF4), but with significantly low bias (mean bias by a factor of 2). The simulated difference  
253 in AOD magnitude is similar to that found by Zhang et al. (2014) over the northern sub-Saharan African. Using the  
254 QFEDv2.4 fire emission, the simulated regional mean AOD is a factor of 1.5 higher than that using the GFEDv3.1  
255 emission in their study. Relatively good performance of S\_QF is also seen over Mexico. The simulated time  
256 evolution agrees well with AERONET retrievals except for small discrepancies (e.g. during Apr.17 -19). A better  
257 agreement with the AERONET retrievals is found for the NRL data than MACC reanalysis at both sites. Consistent  
258 with the evaluation using reanalysis, the simulated temporal evolution of AOD during Apr. 1-10 agrees well with  
259 both reanalysis data and AERONET retrievals in selected regions. This gives us further confidence in choosing this  
260 period for further investigation.

261 The model is further evaluated against the IMPROVE data for BC and POM mass concentrations (Fig. 5). In the  
262 downwind region, the simulated mass concentrations in simulation S\_QF lie within a factor of 2 of the observed  
263 values at most sites. However, the magnitude is generally underestimated in simulations with the GFED emissions  
264 (S\_GF3 and S\_GF4), especially in S\_GF3. BC and POM concentrations in the downwind regions are affected by



265 transport of aerosols from Southern Mexico (Fig. S3). A larger amount of fire emission in Southern Mexico would  
266 result in a higher BC (POM) concentration in the downwind region. This explains the slightly higher concentrations  
267 in the simulation S\_GF4 than S\_GF3, as BC and POM emissions over Southern Mexico are higher in GFED v4.1  
268 due to the inclusion of small fires (Randerson et al., 2012). The good agreement between S\_QF and observations  
269 suggests that the QFED data have a reasonable total emission rate. However, in the source region, the simulation  
270 S\_QF displays large positive bias with a large majority of the values fall out of the a-factor-of-2 band. Given the  
271 reasonable total emission rate in QFED and a good agreement of AOD with AERONET retrievals at Cart\_site, this  
272 might result from the discrepancies in the vertical distribution the fire emissions. Fire-emitted BC and POM in  
273 simulations S\_QF and S\_GF3 reach maximum values in the lowest level and decrease sharply to the next level,  
274 while low-level fire emissions in S\_GF4 distribute in a more uniform way (Fig. S4). As the sampling was done on  
275 the lowest model level at most sites to compare with the IMPROVE data, this explains the strong overestimation in  
276 S\_QF. Although the same impact from vertical distribution of fire emission also appears in simulation S\_GF3, it is  
277 partly offset by its negative bias in the total emission rate.

## 278 **3.2 10-day Mean Results**

279 Given the good model performance during Apr 1-10, we proceed to analyze the short-term effects of fire aerosols  
280 during this period with nudged ensemble simulations. We define “fire AOD” as the AOD difference between the  
281 simulations with and without fire emissions.

### 282 **3.2.1 Fire Aerosol Distribution**

283 Fig. 6 shows the spatial distributions of 10-day average ensemble mean fire AOD. For reference, the total AOD  
284 in the simulation without fire emissions is shown in Fig. S2. During the period, regional mean AOD increases by  
285 6.4% (E\_GF3), 6.4% (E\_GF4) and 70.2% (E\_QF) in the central U.S. and 10.4% (E\_GF3), 13.3% (E\_GF4), and  
286 49.6% (E\_QF) in Southern Mexico when fire emissions are included. In E\_QF, high fire AOD covers almost the  
287 entire selected region and extends further north. Maximum values of fire AOD stay above 0.2 around the Yucatan  
288 Peninsula. Over the Central U.S, significant fire AOD ranging between 0.04 and 0.1 appears in the southwest part of  
289 the selected region. Apart from the significant AOD difference in selected regions, large fire AOD also appears near  
290 the eastern coast as a result of local fire emission and the eastward transport of fire aerosols from both regions.  
291 Overall, the modeled fire AOD is much smaller in simulations with GFED emissions.

### 292 **3.2.2 Fire Aerosol Radiative Effect**

293 As described in Sect. 2.4, fire aerosol radiative effect can be decomposed into three items including fire aerosol  
294 DRE, fire aerosol CRE and fire aerosol surface albedo effect (Table S3). Fig.7 shows the spatial distributions of  
295 shortwave direct effect (SDRE) and shortwave cloud radiative effect (SCRE). They are major contributors to the  
296 total fire aerosol forcing in the selected regions. For reference, total aerosol forcing and total shortwave cloud  
297 forcing in the simulation without fire emissions are shown in Fig. S2. The spatial distribution of SDRE and SCRE  
298 are similar for the three cases, but with different magnitudes and statistical significant regions for simulations with

299 QFED and GFED fire emissions. In the Central U.S., fire aerosol SDRE is negligible in GFED forced simulations  
300 due to small fire AOD. Although the fire AOD is larger in simulation E\_QF, the compensation between warming  
301 effect of fire BC and cooling effect of fire POM still results a weak forcing of about  $-0.1W m^{-2}$ . Over southern  
302 Mexico, all simulations produce significant cooling by fire aerosol SCRE with maximum values three times as large  
303 as those of corresponding SDRE. For both SDRE and SCRE, the largest fire aerosol effects appear in the E\_QF  
304 simulation while the E\_GF3 yields the weakest forcing, which is consistent with the modeled fire AOD in these  
305 simulations.

306 In the following analysis, we will focus on the results from the E\_QF simulation. Both SDRE and SCRE spread  
307 outside the two selected regions and extend eastward reaching coast regions. A stronger fire aerosol effect is seen in  
308 the Southern Mexico region. Strong SDRE appears over the Yucatan Peninsula where fire AOD peaks (Fig. 6).  
309 Regional mean 10-day average of SDRE and SCRE reach  $-0.86 W m^{-2}$  and  $-3.02W m^{-2}$  respectively. It's interesting  
310 to note that the maximum SCRE tends to center around adjacent Gulf of Mexico rather than the land region. In the  
311 central U.S, despite moderate fire aerosol SDRE, a positive SCRE exceeding  $2W m^{-2}$  appears in the north part of the  
312 region while a comparable negative SCRE appears in the south part of the region

313 To find out the causes of the fire aerosol SCRE, fire aerosol-induced changes in cloud properties are analyzed.  
314 Given the largely insignificant change in cloud fraction (Fig. 8), the negative fire aerosol SCRE in both regions is  
315 mainly associated with increases in liquid water path (LWP) and droplet number concentrations (CDNC). The  
316 increased CDNC due to an increase of CCN from fire aerosols (Fig. 8) leads to smaller droplet sizes, which in turn  
317 increase cloud albedo by enhancing backscattering (Twomey, 1977) and further affect LWP by decreasing  
318 precipitation efficiency and allowing more liquid water to accumulate (Albrecht, 1989; Ghan et al., 2012). These  
319 changes in warm cloud properties demonstrate important contributions of both aerosol first and second indirect  
320 effects to the negative SCRE. Over Southern Mexico, although changes of CDNC and LWP are of comparable  
321 magnitudes between Gulf of Mexico and the land region (Fig.8), relative changes of both items are much larger over  
322 Gulf of Mexico (Fig.S5) due to the smaller magnitudes of background CDNC and LWP here (Fig. S6), which tend  
323 to lead to a more sensitive response of SCRE. That's why the maximum SCRE over Southern Mexico is more  
324 centered around Gulf of Mexico. Changes in ice water path (IWP) and ice crystal number concentration (ICNC) can  
325 also significantly affect SCRE, but with an opposite sign and mostly in the central U.S. The decreased IWP and  
326 ICNC, which are possibly caused by fire aerosol-induced changes in the circulation (Ten Hoeve et al, 2012) and  
327 reduced coarse mode dust aerosol concentrations (Fig.S7), are responsible for the positive SCRE and the negative  
328 longwave cloud radiative effect (Table S3) in the north part of central U.S. In the south part of central U.S., the  
329 reduction of IWP and ICNC also results in a positive SCRE, which partly offsets the negative SCRE resulting from  
330 changes in warm cloud properties. This explains the weaker total negative SCRE in this region compared to the  
331 Southern Mexico region despite the more substantial increase in CDNC and LWP here. In the northeast of the  
332 extended coastal regions, a more significant change of LWP comparable to that in the central U.S appears, while a  
333 more significant change of CDNC comparable to that in Southern Mexico occurs in the southwest. The combined  
334 effect leads to the total fire aerosol effect in the extended regions.

335 The ensemble method provides another effective way to distinguish fire aerosol radiative effect by comparing  
336 the radiative forcing distribution of ensemble members between simulation with and without fire emission. A  
337 significant difference in the distribution of total aerosol (cloud) forcing indicates a significant fire aerosol direct  
338 (cloud) effect. As shown in Fig. 9, a shift towards stronger magnitude occurs to the total aerosol forcing when fire  
339 aerosols are considered. Simulation E\_QF has a larger percentage of grid cells with SDRE below  $-4.2\text{W m}^{-2}$ , while  
340 more grid cells exceed  $-4.2\text{W m}^{-2}$  in E\_NF, which indicates a significant negative fire aerosol direct effect. The same  
341 shift also appears to the total shortwave cloud forcing with more grid cells having shortwave cloud forcing below  $-$   
342  $30\text{W m}^{-2}$  in the simulation E\_QF. Regional mean total aerosol and shortwave cloud forcing in southern Mexico  
343 become more negative ( $-0.86$  and  $-3.02\text{ W m}^{-2}$ ) with fire aerosols.

344 Fig. 10 illustrates ensemble behavior of 10-day average regional mean total aerosol and cloud forcing from all  
345 simulations as well as resulted fire aerosol SDRE and SCRE. The GFED forced simulations not only resemble in  
346 ensemble mean, but also have small difference in ensemble member distribution. Although members in the E\_QF  
347 simulation capture stronger aerosol forcing, thus stronger fire aerosol SDRE than those in E\_GF3 and E\_GF4, the  
348 ensemble spread (as indicated by the maximum and minimum values) in the three simulations is similar. Moreover,  
349 the E\_QF simulation yields a smaller spread of SCRF compared with the GFED forced simulations despite a  
350 stronger ensemble mean SCRF. In each fire simulation, ensemble mean fire aerosol SCRE has a much larger  
351 magnitude than SDRE. So is the corresponding ensemble spread. Taking results from E\_QF simulation as an  
352 example, ensemble spread of SCRE reaches  $0.47\text{ W m}^{-2}$ , accounting for 15.6% of the corresponding ensemble mean,  
353 while ensemble spread of SDRE is  $0.03\text{W m}^{-2}$  accounting for 3.5% of the corresponding ensemble mean.

### 354 3.3 Daily RF

355 The fire aerosol effect is also investigated for individual days. The spatial distributions of SDRF and SCRF on April  
356 7 are shown in Fig 11, when relatively high fire emissions appear in both regions. Negative fire aerosol SDRE  
357 appears in the central U.S. biomass-burning region indicating the dominant role of POM scattering. Fire aerosol  
358 SDRE over Southern Mexico shows a contrast of warming effect in land region and cooling effect in adjacent ocean  
359 despite similar aerosol loading in the two regions. However, they do have nearly equal clear-sky BC absorption and  
360 POM scattering (Fig. 12). Difference in low-level cloud distributions between two regions leads to different signs of  
361 the simulated all-sky SDRE. Over land, when clouds appear under elevated aerosol layers, more solar radiation is  
362 reflected back to space and this leads to amplified BC absorption and more positive direct aerosol forcing (Keil and  
363 Haywood, 2003; Zhang et al., 2016; Jiang et al., 2016). In contrast, neither absorption nor scattering changes  
364 significantly from clear-sky to all-sky condition over adjacent areas over the ocean, since the small cloud fraction is  
365 small. Same enhanced absorption of above-cloud aerosols is also found over the west Atlantic Ocean. Fire aerosols  
366 produce remarkable negative SCRE up to  $-16\text{W m}^{-2}$  over Southern Mexico land in response to the increase in CDNC  
367 and LWP.

### 368 3.4 Discussion about Simulation Strategy

369 Fig. 13 shows the daily variation of the regional mean total (direct) aerosol forcing and cloud forcing. Both the  
370 ensemble mean and spread are investigated here. The total aerosol forcing exhibits considerable diversity across  
371 ensemble members within each simulation even though the simulated AOD is nearly indistinguishable (Fig. 3).  
372 Taking results from simulation E\_QF as an example, maximum values of difference between members exceed 0.4  
373  $W m^{-2}$  for aerosol forcing and  $5W m^{-2}$  for cloud forcing, which are approximate 10% of the corresponding ensemble  
374 mean values. The large spread of total aerosol forcing and cloud forcing will lead to uncertainties in the estimation  
375 of fire aerosol effect. This points out the importance of conducting ensemble simulations in order to get a more  
376 comprehensive estimate of daily fire aerosol effect. The minimum ensemble size required for this case is  
377 investigated in terms of the ensemble mean and spread estimate. Simulated ensemble mean fire aerosol SDRE  
378 remains nearly unchanged regardless of the ensemble size (Fig. 14a). However, discrepancies in the ensemble mean  
379 fire aerosol SCRF (Fig. 14b) are substantial when the number of ensemble members is small. The same is true for  
380 the ensemble spread of fire aerosol SCRF (Fig. S8). In order to quantify the discrepancies of the simulated SCRE,  
381 we chose the ensemble mean SCRE in the 20-member simulation as a reference and use the root mean square errors  
382 (RMSE) of the ensemble mean SCRE in the N-member simulation to quantify the deviation of the simulated SCRE  
383 from the reference value. It is calculated as the standard deviation of the differences between the daily ensemble  
384 mean SCRE in the N-member simulation and the 20-member simulation. For each N, we randomly sampled 1000  
385 times from the 20 members to help reduce the influence from limited sampling. Figure 15 shows that both the  
386 RMSE of ensemble mean SCRE and the difference of RMSE between the 1000 groups of simulations (for each N)  
387 decrease with increasing N. The minimum number of N required is determined when the 90<sup>th</sup> percentile of RMSE is  
388 smaller than a threshold RMSE. Without a good reference, we set the threshold RMSE to 20% ( $0.566Wm^{-2}$ ) of the  
389 reference 10-day mean SCRE ( $-2.83Wm^{-2}$ ). As shown in Fig.15, at least 11 members are needed to meet this  
390 criterion.

391 Fire aerosol sources are often intermittent and height-dependent and there is a need to estimate the short-term  
392 effective aerosol forcing. Although nudging helps to constrain large-scale features, the simulated cloud properties  
393 (e.g. cloud fraction and LWP) and their response to aerosol changes can still be sensitive to small perturbations in  
394 the atmospheric state. Therefore, for investigating the short-term aerosol effect, a single simulation might not be  
395 sufficient to tell whether the aerosol effect is significant. The use of ensembles provides an effective way to estimate  
396 the uncertainty. Previous investigations of short-term fire aerosol effect are mainly based on single-member  
397 simulations (Wu et al., 2011; Sena et al., 2013; Kolusu et al., 2015). While this might be less a problem for SDRE,  
398 one should be more careful when investigating the aerosol indirect effect and conduct ensemble simulations to see  
399 whether the estimated fire aerosol effects are robust.

#### 400 4. Summary

401 In this study, we investigated the short-term effect of fire aerosols on cloud and radiation using CAM5  
402 simulations. Month-long single-member simulations and 10-day ensemble simulations were conducted in April,  
403 2009. In order to help extract signals on short time scales, we used nudging to constrain horizontal winds in all  
404 simulations. Our investigation focused on Southern Mexico where there were constant intensive fire activities and

405 the Central U.S. with occasionally large fires. Apart from the local effect, fire emissions from the two regions are  
406 shown to affect downwind coastal regions through transport.

407 Modeled AOD and mass concentrations (BC and POM) were evaluated against observations. In general, all  
408 simulations with fire emissions reproduce the observed temporal variation of daily mean AOD well, although the  
409 simulated magnitude is smaller. The model performance is better when QFEDv2.4 is used, which has larger fire  
410 emissions. Modeled regional mean AOD values in simulations using two versions of GFED fire emission data are  
411 barely distinguishable, despite the inclusion of small fires and changed injection heights in GFEDv4.1 used in this  
412 study. Both simulate about a factor of 1.5 smaller AOD than that in the simulation using the QFED fire emissions.  
413 At sites in the downwind region, the modeled BC and POM mass concentrations in the simulation with QFEDv2.4  
414 emission (S\_QF) agree well with the IMPROVE data. In contrast, simulations with the other two fire emission  
415 datasets (S\_GF3 and S\_GF4) have a low bias. The simulated AOD in the source region in S\_QF also agrees well  
416 with the AERONET data (Cart\_Site). If there is no large compensating error in the model, QFEDv2.4 seems more  
417 reasonable in terms of the total (vertically-integrated) emission rate. On the other hand, S\_QF strongly overestimates  
418 BC and POM concentrations in the source region. Considering that the source-region AOD and the downwind  
419 surface mass concentrations are well simulated, the overestimation suggests the actual emission peak might appear  
420 at higher levels compared to the height-dependent injection rates applied in the S\_QF simulation.

421 Based on the evaluation, we chose the first 10 days as the simulation period and focused on the simulation with  
422 QFEDv2.4 fire emission in our ensemble nudged simulations. In our method, the nudged ensembles are generated  
423 by adding a very weak temperature nudging along with horizontal-wind nudging and perturbing the nudging time  
424 scale of temperature gently. In this way, small temperature perturbations are added to the simulation at each time  
425 step, while the large-scale circulation features are very similar between individual members. We first investigated  
426 the 10-day mean effective fire aerosol forcing. Decomposition of total aerosol radiative forcing shows that fire  
427 aerosol effects in the two selected regions are dominated by the SCRE. All fire simulations show similar spatial  
428 distribution of SDRE and SCRE, but with different magnitudes and statistically significant regions. The similarity in  
429 the spatial distribution is expected since the three emission datasets differ mainly in the emission magnitude and no  
430 much in spatial distribution in the focus regions of this study. Fire aerosol effects in simulations with GFED  
431 emissions (E\_GF3 and E\_GF4) are weaker than that with QFEDv2.4 emission (E\_QF) by a factor of 1.5 for SCRE  
432 and a factor of more than 4 for SDRE. Overall, the difference in simulated AOD and fire aerosol indirect radiative  
433 effects between simulations is smaller compared to the difference between fire emissions, consistent with the  
434 findings in sub-Saharan African biomass-burning region (Zhang et al. 2014).

435 Fire aerosols produce a negative direct effect of  $-0.1 \text{ W m}^{-2}$  in the Central U.S. and  $-0.86 \text{ W m}^{-2}$  in Southern  
436 Mexico in E\_QF during the 10-day period. Within each region, negative fire aerosol SDRE peaks where fire AOD  
437 reaches maximum. Unlike the limited area affected by significant fire aerosol SDRE, fire aerosol SCRE from  
438 selected regions spreads eastward and northward, affecting remote coast regions. Ensemble mean results show  
439 strong SCRE over almost the entire Southern Mexico, with a 10-day regional mean value of  $-3.02 \text{ W m}^{-2}$ . Over the  
440 central U.S., the SCRE is positive in the north and negative in the south and the regional mean is small ( $-$   
441  $0.56 \text{ W m}^{-2}$ ). Maximum SCRE stays below  $-4 \text{ W m}^{-2}$  in the (south) central U.S. and  $-10 \text{ W m}^{-2}$  in Southern

442 Mexico in response to significantly increased LWP and CDNC. Decreases of IWP and ICNC also contribute to fire  
443 aerosol SCRE in the Central U.S. but with an opposite sign. The offset effect of the positive forcing induced by  
444 changes in cloud ice properties explains the smaller SCRE in the central U.S. despite the larger changes in cloud  
445 droplet properties.

446 We also investigated fire aerosol effects on the daily time scale, where the variation in the simulated fire aerosol  
447 effect can be large among the ensemble members. The large ensemble spread of total aerosol and cloud forcing  
448 indicates large uncertainties in estimating daily fire aerosol effects, despite similar AOD across ensemble members.  
449 Further investigations show that the simulated ensemble mean and spread with less than 7 members differs  
450 considerably to those with more members. Our results suggest that for short-term simulations of aerosol and cloud  
451 processes, even small perturbations might result in large difference across members despite constrained large scale  
452 features. In order to obtain a robust estimate of the effective fire aerosol forcing during a short period, it is important  
453 to conduct ensemble simulations with sufficient ensemble members.

454

455

## 456 **Acknowledgments**

457 We thank two anonymous reviewers for their careful reviews and suggestions that helped to greatly improve the  
458 analyses and discussion presented in this paper. This study was supported by the U.S. Department of Energy  
459 (DOE)'s office of Science as part of the Regional and Global Climate Modeling Program (NSF-DOE-USDA  
460 EaSM2). The work was also supported by the National Natural Science Foundation of China (NSFC) under Grants  
461 No. 41621005 and 41330420, the National Key Basic Research Program (973 Program) of China under Grant No.  
462 2010CB428504, and the Jiangsu Collaborative Innovation Center of Climate. The Pacific Northwest National  
463 Laboratory (PNNL) is operated for DOE by Battelle Memorial Institute under contract DE-AC05-76RL01830.  
464 Computations were performed using resources of the National Energy Research Scientific Computing Center  
465 (NERSC) at Lawrence Berkeley National Laboratory and PNNL Institutional computing. All model results are  
466 available from the corresponding author upon request.

467 **References:**

- 468 Albrecht, B. A.: Aerosols, cloud microphysics, and fractional cloudiness, *Science*, 245, 1227-1231, 1989.
- 469 Benedetti, A., Morcrette, J. J., Boucher, O., Dethof, A., Engelen, R., Fisher, M., Flentje, H., Huneeus, N., Jones, L.,  
470 and Kaiser, J.: Aerosol analysis and forecast in the European centre for medium-range weather forecasts integrated  
471 forecast system: 2. Data assimilation, *Journal of Geophysical Research: Atmospheres*, 114, 2009.
- 472 Bond, T. C., Doherty, S. J., Fahey, D., Forster, P., Berntsen, T., DeAngelo, B., Flanner, M., Ghan, S., Kärcher, B.,  
473 and Koch, D.: Bounding the role of black carbon in the climate system: A scientific assessment, *Journal of*  
474 *Geophysical Research: Atmospheres*, 118, 5380-5552, 2013.
- 475 Bony, S., Colman, R., Kattsov, V. M., Allan, R. P., Bretherton, C. S., Dufresne, J.-L., Hall, A., Hallegatte, S.,  
476 Holland, M. M., and Ingram, W.: How well do we understand and evaluate climate change feedback processes?,  
477 *Journal of Climate*, 19, 3445-3482, 2006.
- 478 Boucher, O., Randall, D., Artaxo, P., Bretherton, C., Feingold, G., Forster, P., Kerminen, V.-M., Kondo, Y., Liao,  
479 H., and Lohmann, U.: Clouds and aerosols, in: *Climate change 2013: the physical science basis. Contribution of*  
480 *Working Group I to the Fifth Assessment Report of the Intergovernmental Panel on Climate Change*, Cambridge  
481 University Press, 571-657, 2013.
- 482 Brito, J., Rizzo, L. V., Morgan, W. T., Coe, H., Johnson, B., Haywood, J., Longo, K., Freitas, S., Andreae, M. O.,  
483 and Artaxo, P.: Ground-based aerosol characterization during the South American Biomass Burning Analysis  
484 (SAMBBA) field experiment, *Atmospheric Chemistry and Physics*, 14, 12069-12083, 2014.
- 485 Chen, D., Liu, Z., Schwartz, C. S., Lin, H.-C., Cetola, J. D., Gu, Y., and Xue, L.: The impact of aerosol optical depth  
486 assimilation on aerosol forecasts and radiative effects during a wild fire event over the United States, *Geoscientific*  
487 *Model Development*, 7, 2709-2715, 2014.
- 488 Chubarova, N., Nezval, Y., Sviridenkov, I., Smirnov, A., and Slutsker, I.: Smoke aerosol and its radiative effects  
489 during extreme fire event over Central Russia in summer 2010, *Atmospheric Measurement Techniques*, 5, 557-568,  
490 2012.
- 491 Chubarova, N. Y., Prilepsky, N. G., Rublev, A. N., and Riebau, A. R.: A Mega-Fire event in central Russia: fire  
492 weather, radiative, and optical properties of the atmosphere, and consequences for subboreal forest plants,  
493 *Developments in environmental science*, 8, 247-264, 2008.
- 494 Dee, D., Uppala, S., Simmons, A., Berrisford, P., Poli, P., Kobayashi, S., Andrae, U., Balmaseda, M., Balsamo, G.,  
495 and Bauer, P.: The ERA-Interim reanalysis: Configuration and performance of the data assimilation system,  
496 *Quarterly Journal of the royal meteorological society*, 137, 553-597, 2011.
- 497 Eskes, H., Huijnen, V., Arola, A., Benedictow, A., Blechschmidt, A.-M., Botek, E., Boucher, O., Bouarar, I.,  
498 Chabrilat, S., and Cuevas, E.: Validation of reactive gases and aerosols in the MACC global analysis and forecast  
499 system, *Geoscientific model development*, 8, 3523-3543, 2015.

500 Ghan, S. J., Liu, X., Easter, R. C., Zaveri, R., Rasch, P. J., Yoon, J.-H., and Eaton, B.: Toward a minimal  
501 representation of aerosols in climate models: Comparative decomposition of aerosol direct, semidirect, and indirect  
502 radiative forcing, *Journal of Climate*, 25, 6461-6476, 2012.

503 Ghan, S. J.: Technical Note: Estimating aerosol effects on cloud radiative forcing, *Atmos. Chem. Phys.*, 13, 9971-  
504 9974, doi:10.5194/acp-13-9971-2013, 2013.

505 Giglio, L., Randerson, J. T., and van der Werf, G. R. (2013), Analysis of daily, monthly, and annual burned area  
506 using the fourth-generation global fire emissions database (GFED4) *J. Geophys. Res. Biogeosci.*, 118, 317–328,  
507 doi:10.1002/jgrg.20042.

508 Holben, B. N., Eck, T., Slutsker, I., Tanre, D., Buis, J., Setzer, A., Vermote, E., Reagan, J., Kaufman, Y., and  
509 Nakajima, T.: AERONET—A federated instrument network and data archive for aerosol characterization, *Remote  
510 sensing of environment*, 66, 1-16, 1998.

511 Iacono, M. J., Delamere, J. S., Mlawer, E. J., Shephard, M. W., Clough, S. A., and Collins, W. D.: Radiative forcing  
512 by long-lived greenhouse gases: Calculations with the AER radiative transfer models, *Journal of Geophysical  
513 Research: Atmospheres*, 113, 2008.

514 Jacobson, M. Z.: Effects of biomass burning on climate, accounting for heat and moisture fluxes, black and brown  
515 carbon, and cloud absorption effects, *Journal of Geophysical Research: Atmospheres*, 119, 8980-9002, 2014.

516 Jiang, Y., Lu, Z., Liu, X., Qian, Y., Zhang, K., Wang, Y., and Yang, X.-Q.: Impacts of global open-fire aerosols on  
517 direct radiative, cloud and surface-albedo effects simulated with CAM5, *Atmospheric Chemistry and Physics  
518 (Online)*, 16, 2016.

519 Kaufman, Y. J., Koren, I., Remer, L. A., Rosenfeld, D., and Rudich, Y.: The effect of smoke, dust, and pollution  
520 aerosol on shallow cloud development over the Atlantic Ocean, *Proceedings of the National Academy of Sciences of  
521 the United States of America*, 102, 11207-11212, 2005.

522 Keil, A., and Haywood, J. M.: Solar radiative forcing by biomass burning aerosol particles during SAFARI 2000: A  
523 case study based on measured aerosol and cloud properties, *Journal of Geophysical Research: Atmospheres*, 108,  
524 2003.

525 Kolusu, S., Marsham, J., Mulcahy, J., Johnson, B., Dunning, C., Bush, M., and Spracklen, D.: Impacts of Amazonia  
526 biomass burning aerosols assessed from short-range weather forecasts, *Atmospheric Chemistry and Physics*, 15,  
527 12251-12266, 2015.

528 Kooperman, G. J., Pritchard, M. S., Ghan, S. J., Wang, M., Somerville, R. C., and Russell, L. M.: Constraining the  
529 influence of natural variability to improve estimates of global aerosol indirect effects in a nudged version of the  
530 Community Atmosphere Model 5, *Journal of Geophysical Research: Atmospheres*, 117, 2012.

531 Korontzi, S., McCarty, J., Loboda, T., Kumar, S., and Justice, C.: Global distribution of agricultural fires in  
532 croplands from 3 years of Moderate Resolution Imaging Spectroradiometer (MODIS) data, *Global Biogeochemical  
533 Cycles*, 20, 2006.



534 Lin, N.-H., Tsay, S.-C., Maring, H. B., Yen, M.-C., Sheu, G.-R., Wang, S.-H., Chi, K. H., Chuang, M.-T., Ou-Yang,  
535 C.-F., and Fu, J. S.: An overview of regional experiments on biomass burning aerosols and related pollutants in  
536 Southeast Asia: From BASE-ASIA and the Dongsha Experiment to 7-SEAS, *Atmospheric Environment*, 78, 1-19,  
537 2013.

538 Liu, X., Easter, R. C., Ghan, S. J., Zaveri, R., Rasch, P., Shi, X., Lamarque, J.-F., Gettelman, A., Morrison, H., and  
539 Vitt, F.: Toward a minimal representation of aerosols in climate models: Description and evaluation in the  
540 Community Atmosphere Model CAM5, *Geoscientific Model Development*, 5, 709, 2012.

541 Liu, X.: Impacts of global open-fire aerosols on direct radiative, cloud and surface-albedo effects simulated with  
542 CAM5, *Atmos. Chem. Phys*, 1680, 7324, 2016.

543 Lu, Z., and Sokolik, I. N.: The effect of smoke emission amount on changes in cloud properties and precipitation: A  
544 case study of Canadian boreal wildfires of 2007, *Journal of Geophysical Research: Atmospheres*, 118, 2013.

545 Magi, B., Rabin, S., Shevliakova, E., and Pacala, S.: Separating agricultural and non-agricultural fire seasonality at  
546 regional scales, *Biogeosciences*, 9, 3003, 2012.

547 Malm, W. C., Schichtel, B. A., Pitchford, M. L., Ashbaugh, L. L., and Eldred, R. A.: Spatial and monthly trends in  
548 speciated fine particle concentration in the United States, *Journal of Geophysical Research: Atmospheres*, 109,  
549 2004.

550 Mlawer, E. J., Taubman, S. J., Brown, P. D., Iacono, M. J., and Clough, S. A.: Radiative transfer for inhomogeneous  
551 atmospheres: RRTM, a validated correlated-k model for the longwave, *Journal of Geophysical Research:*  
552 *Atmospheres*, 102, 16663-16682, 1997.

553 Morrison, H., and Gettelman, A.: A new two-moment bulk stratiform cloud microphysics scheme in the Community  
554 Atmosphere Model, version 3 (CAM3). Part I: Description and numerical tests, *Journal of Climate*, 21, 3642-3659,  
555 2008.

556 Mu, M., Randerson, J., van der Werf, G., Giglio, L., Kasibhatla, P., Morton, D., Collatz, G., DeFries, R., Hyer, E.,  
557 and Prins, E.: Daily and hourly variability in global fire emissions and consequences for atmospheric model  
558 predictions of carbon monoxide, 2011.

559 Neale, R. B., Richter, J. H., and Jochum, M.: The impact of convection on ENSO: From a delayed oscillator to a  
560 series of events, *Journal of Climate*, 21, 5904-5924, 2008.

561 Park, S., and Bretherton, C. S.: The University of Washington shallow convection and moist turbulence schemes and  
562 their impact on climate simulations with the Community Atmosphere Model, *Journal of Climate*, 22, 3449-3469,  
563 2009.

564 Randerson, J., Chen, Y., Werf, G., Rogers, B., and Morton, D.: Global burned area and biomass burning emissions  
565 from small fires, *Journal of Geophysical Research: Biogeosciences*, 117, 2012.

566 Reddington, C., Yoshioka, M., Balasubramanian, R., Ridley, D., Toh, Y., Arnold, S., and Spracklen, D.:  
567 Contribution of vegetation and peat fires to particulate air pollution in Southeast Asia, *Environmental Research*  
568 *Letters*, 9, 094006, 2014.

569 Richter, J. H., and Rasch, P. J.: Effects of convective momentum transport on the atmospheric circulation in the  
570 Community Atmosphere Model, version 3, *Journal of Climate*, 21, 1487-1499, 2008.

571 Rubin, J. I., Reid, J. S., Hansen, J. A., Anderson, J. L., Hoar, T. J., Reynolds, C. A., Sessions, W. R., and Westphal,  
572 D. L.: Development of the Ensemble Navy Aerosol Analysis Prediction System (ENAAAPS) and its application of  
573 the Data Assimilation Research Testbed (DART) in support of aerosol forecasting, *Atmospheric Chemistry and  
574 Physics*, 16, 3927, 2016.

575 Sena, E., Artaxo, P., and Correia, A.: Spatial variability of the direct radiative forcing of biomass burning aerosols  
576 and the effects of land use change in Amazonia, *Atmospheric Chemistry and Physics*, 13, 1261-1275, 2013.

577 Smirnov, A., Holben, B., Eck, T., Dubovik, O., and Slutsker, I.: Cloud-screening and quality control algorithms for  
578 the AERONET database, *Remote Sensing of Environment*, 73, 337-349, 2000.

579 Stier, P., Schutgens, N., Bellouin, N., Bian, H., Boucher, O., Chin, M., Ghan, S., Huneeus, N., Kinne, S., and Lin,  
580 G.: Host model uncertainties in aerosol radiative forcing estimates: results from the AeroCom Prescribed  
581 intercomparison study, *Atmospheric Chemistry and Physics*, 13, 3245-3270, 2013.

582 Tarasova, T., Gorchakova, I., Sviridenkov, M., Anikin, P., and Romashova, E.: Estimation of the radiative forcing of  
583 smoke aerosol from radiation measurements at the Zvenigorod scientific station in the summer of 2002, *Izvestiya  
584 Atmospheric and Oceanic Physics*, 40, 454-463, 2004.

585 (Dee et al., 2011), J. E., Jacobson, M. Z., and Remer, L. A.: Comparing results from a physical model with satellite  
586 and in situ observations to determine whether biomass burning aerosols over the Amazon brighten or burn off  
587 clouds, *Journal of Geophysical Research: Atmospheres*, 117, 2012.

588 Tosca, M., Randerson, J., and Zender, C.: Global impact of smoke aerosols from landscape fires on climate and the  
589 Hadley circulation, *Atmospheric Chemistry and Physics*, 13, 5227-5241, 2013.

590 Twomey, S.: The influence of pollution on the shortwave albedo of clouds, *Journal of the atmospheric sciences*, 34,  
591 1149-1152, 1977.

592 van der Werf, G. R., Randerson, J. T., Giglio, L., Collatz, G. J., Mu, M., Kasibhatla, P. S., Morton, D. C., DeFries,  
593 R. S., Jin, Y., and van Leeuwen, T. T.: Global fire emissions and the contribution of deforestation, savanna, forest,  
594 agricultural, and peat fires (1997–2009), *Atmos. Chem. Phys.*, 10, 11707-11735, doi:10.5194/acp-10-11707-2010,  
595 2010.

596 Ward, D., Kloster, S., Mahowald, N., Rogers, B., Randerson, J., and Hess, P.: The changing radiative forcing of  
597 fires: global model estimates for past, present and future, *Atmospheric Chemistry and Physics*, 12, 2012.

598 Wan, H., Rasch, P. J., Zhang, K., Qian, Y., Yan, H., and Zhao, C.: Short ensembles: an efficient method for  
599 discerning climate-relevant sensitivities in atmospheric general circulation models, *Geoscientific Model  
600 Development*, 7, 1961-1977, 2014.

601 Wu, L., Su, H., and Jiang, J. H.: Regional simulations of deep convection and biomass burning over South America:  
602 2. Biomass burning aerosol effects on clouds and precipitation, *Journal of Geophysical Research: Atmospheres*, 116,  
603 2011.

604 Zamora, L. M., Kahn, R., Cubison, M. J., Diskin, G., Jimenez, J., Kondo, Y., McFarquhar, G., Nenes, A., Thornhill,  
605 K., and Wisthaler, A.: Aircraft-measured indirect cloud effects from biomass burning smoke in the Arctic and  
606 subarctic, *Atmospheric Chemistry and Physics*, 16, 715-738, 2016.

607 Zhang, F., Wang, J., Ichoku, C., Hyer, E. J., Yang, Z., Ge, C., Su, S., Zhang, X., Kondragunta, S., and Kaiser, J. W.:  
608 Sensitivity of mesoscale modeling of smoke direct radiative effect to the emission inventory: a case study in  
609 northern sub-Saharan African region, *Environmental Research Letters*, 9, 075002, 2014.

610 Zhang, G. J., and McFarlane, N. A.: Sensitivity of climate simulations to the parameterization of cumulus  
611 convection in the Canadian Climate Centre general circulation model, *Atmosphere-ocean*, 33, 407-446, 1995.

Table 1. List of CAM5 simulations.

Name	Fire emission	Simulation period	Member	Nudging
Group A: Single member simulations				
S_NF	No	January 1- April 30, 2009	1	Horizontal winds (6h)
S_GF3	GFED v3			
S_GF4	GFED v4.1			
S_QF	QFED v2.4			
Group B: Ensemble simulations				
E_NF	No	April 1 - April 10, 2009	10	Horizontal winds (6h) and temperature (~10d)*
E_GF3	GFED v3			
E_GF4	GFED v4.1			
E_QF	QFED v2.4			

\* See section 2.3 for details about ensembles

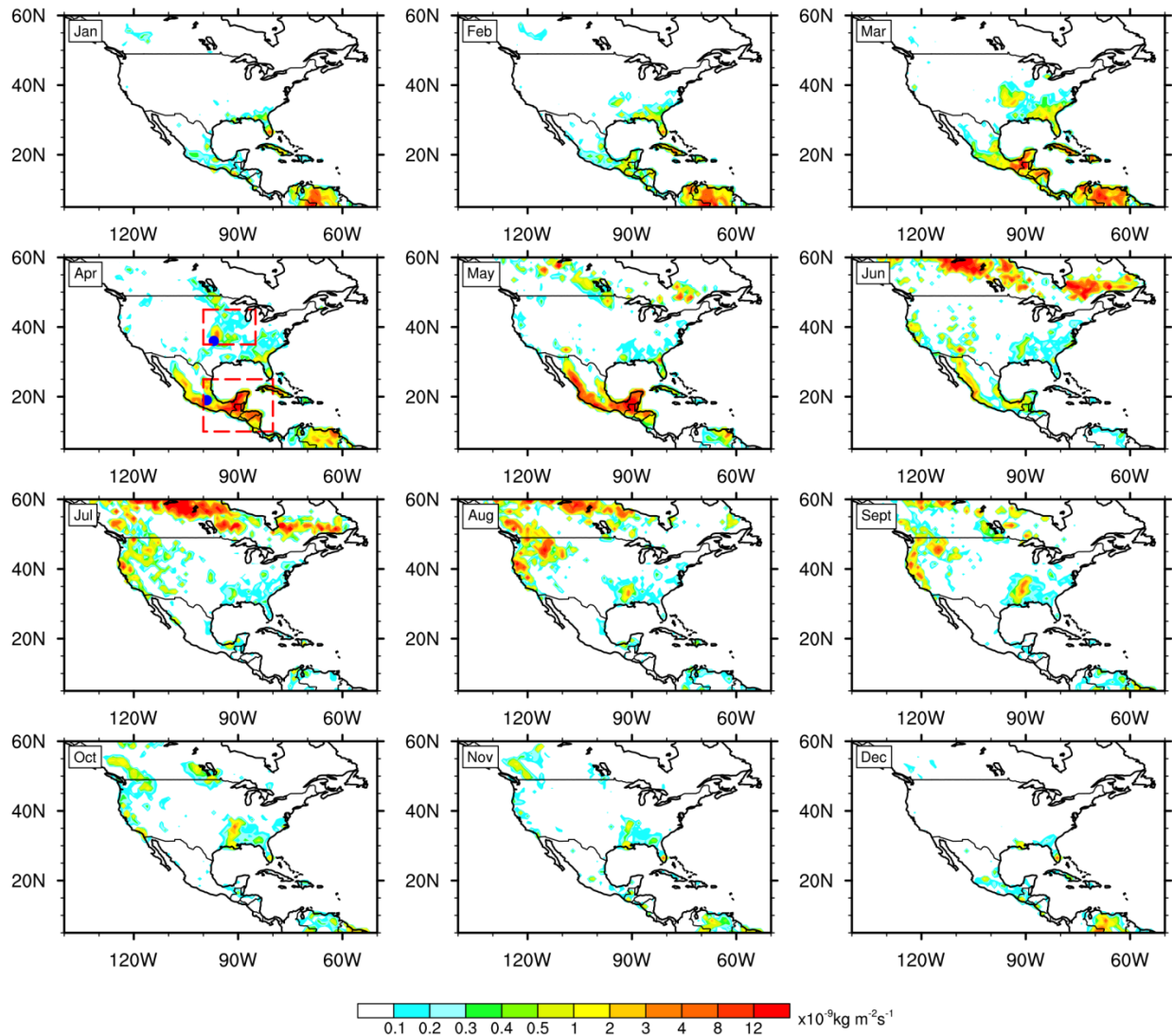


Figure 1. Spatial distributions of multi-year monthly mean biomass burning consumed dry matter over North America during 2003-2014 from GFEDv4.1. Boxes denote selected regions: central U.S. (35 - 45°N, 85 - 100°W) and Southern Mexico (10 - 25°N, 80 - 100°W). Dots denote locations of AERONET sites: Cart\_Site (36°N, 97°W) and Mexico\_City (19°N, 99°W)

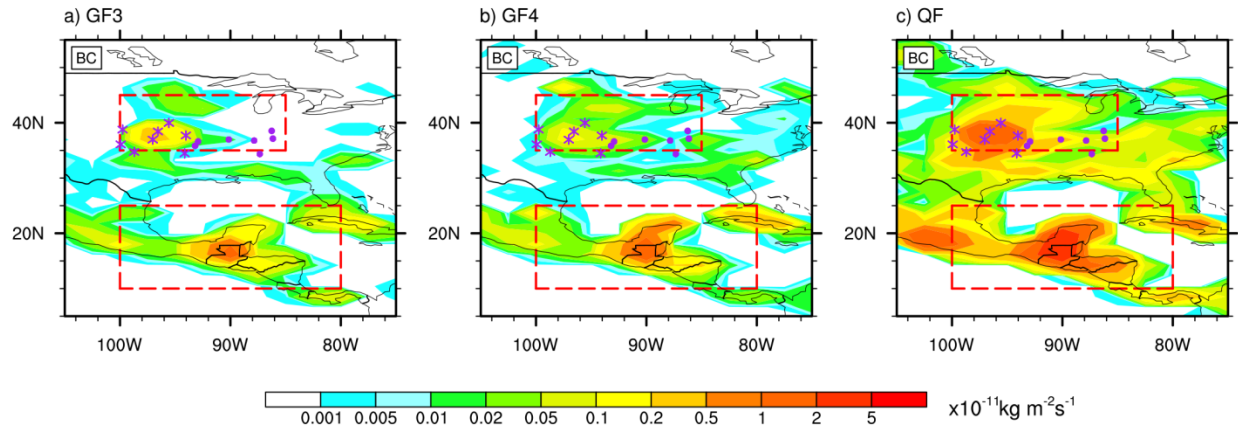


Figure 2. Spatial distributions of monthly mean BC emissions from three emission inventories in April, 2009. IMPROVE data sites are shown as asterisks for sites near the source region and as dots for sites in the region downwind of the fire source.

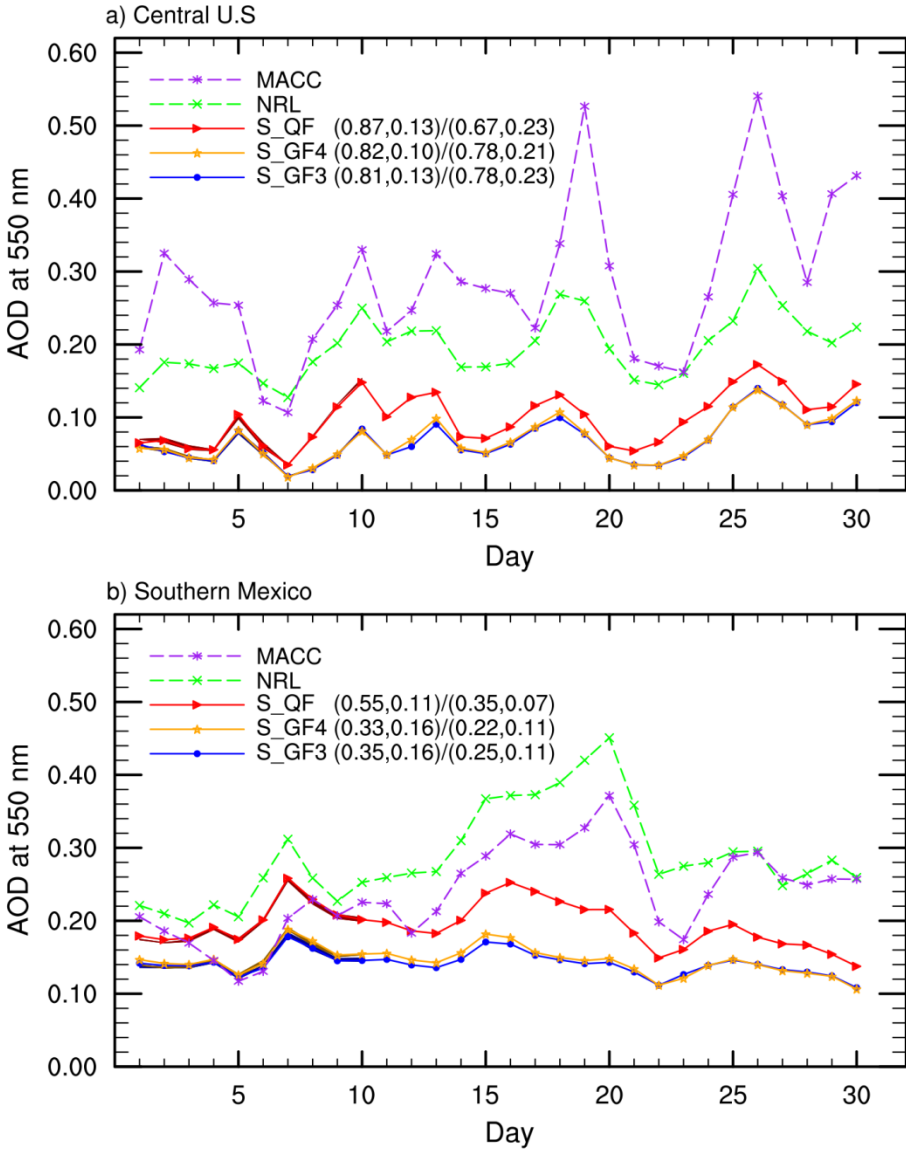


Figure 3. Time series of daily regional mean AOD in April, 2009 in simulations and reanalysis data. Numbers in parenthesis denote time correlation coefficient (TCC) and root mean square error (RMSE) between each simulation in group A and reanalysis data (left: NRL; right: MACC). Individual lines indicate group A simulations. Shaded areas (very narrow) in slightly darker colors during April 1-10 illustrate maximum and minimum values of daily mean AOD among ensemble members in group B simulations. For the single-member simulation and the ensemble simulation driven by same fire emission, the shaded area and the solid line almost overlap, given the barely indistinguishable AOD between ensemble members and the corresponding Group A simulation.

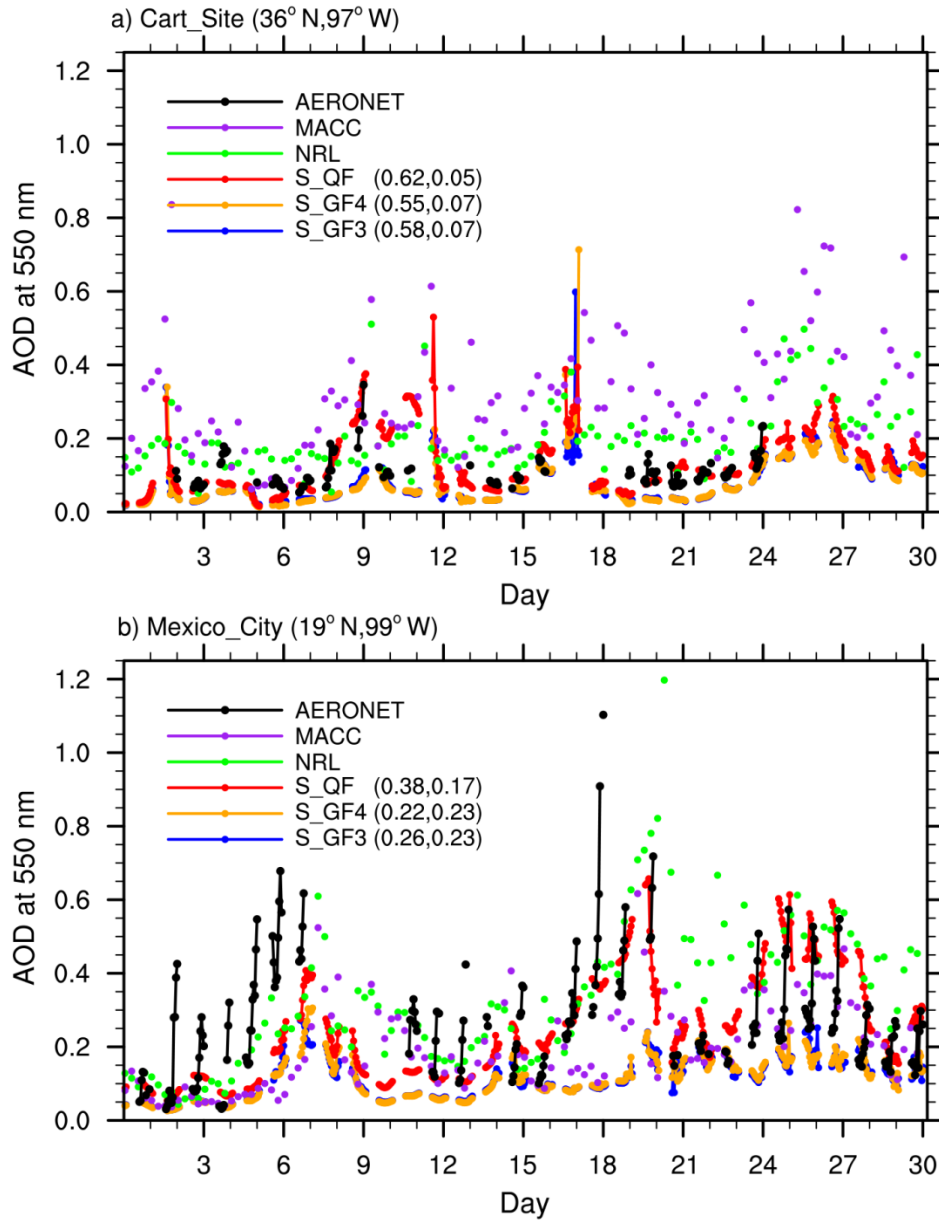


Figure 4. Time series of hourly regional mean AOD in April, 2009 from group A simulations, reanalysis data and AERONET retrievals at AERONET sites. Numbers in parenthesis denote TCC (left) and RMSE (right) between each simulation and AERONET AOD.



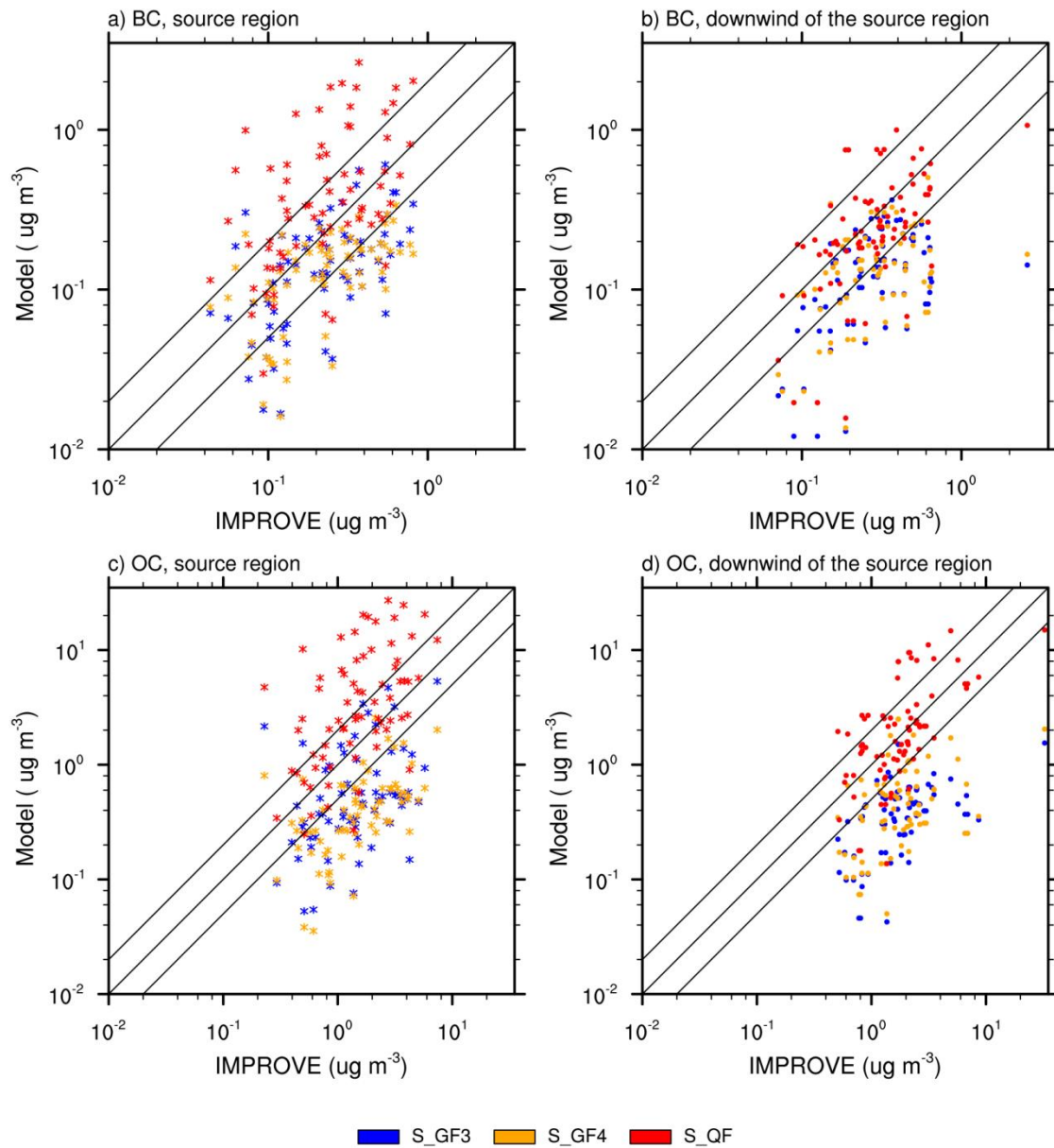


Figure 5. Evaluation of simulated BC (up) and POM (bottom) concentrations in group A simulations against the IMPROVE data at sites near the source and downwind the source region. Locations of these sites are marked with the same symbol in Fig. 2.

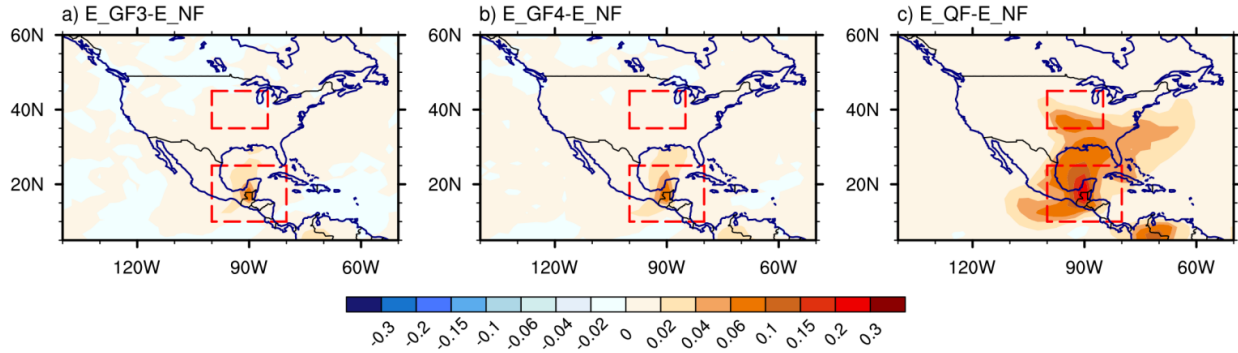


Figure 6. Spatial distributions of 10-day average (Apr. 1-10) ensemble mean AOD differences between simulations with (E\_GF3, E\_GF4, and E\_QF) and without fire emission (E\_NF).

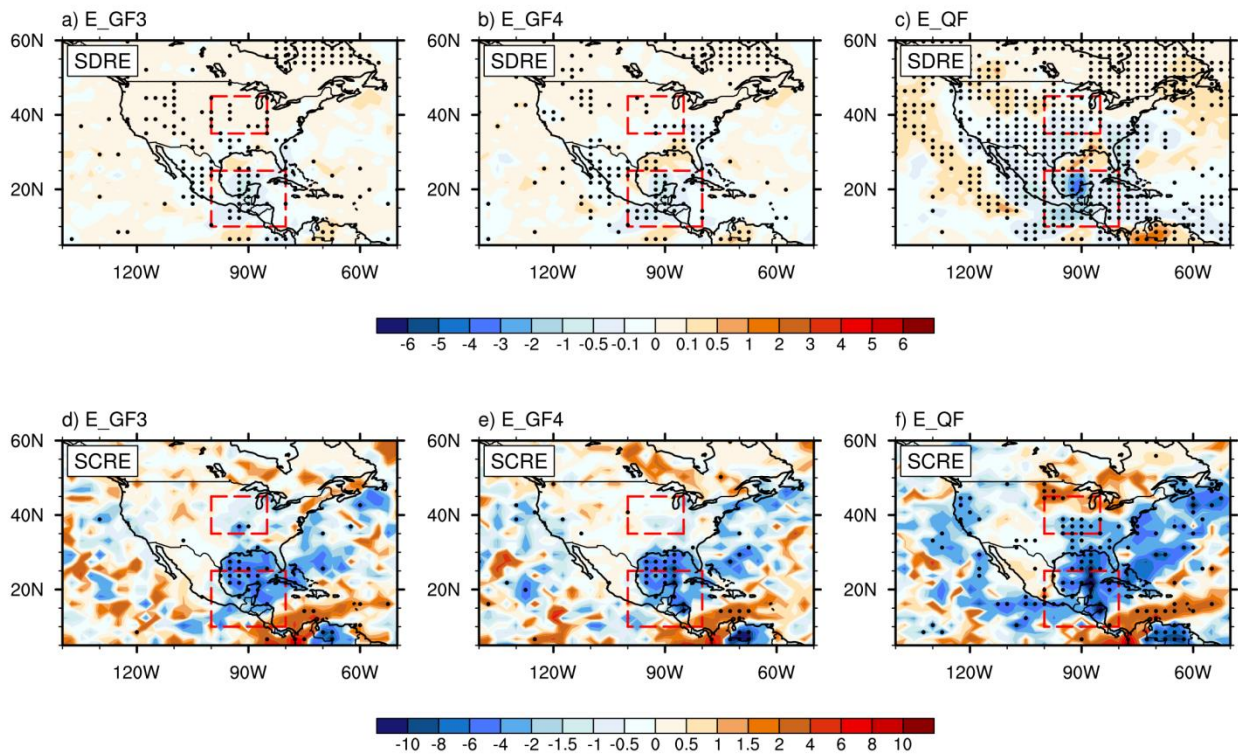


Figure 7. Spatial distributions of 10-day average (Apr. 1-10) ensemble mean fire aerosol shortwave direct radiative effect (SDRE) and shortwave cloud radiative effect (SCRE) ( $W m^{-2}$ ) in group B simulations. Dots denote regions where SDRE is statistically significant at the 95% confidence level based on the Kolmogorov-Smirnov (KS) test.

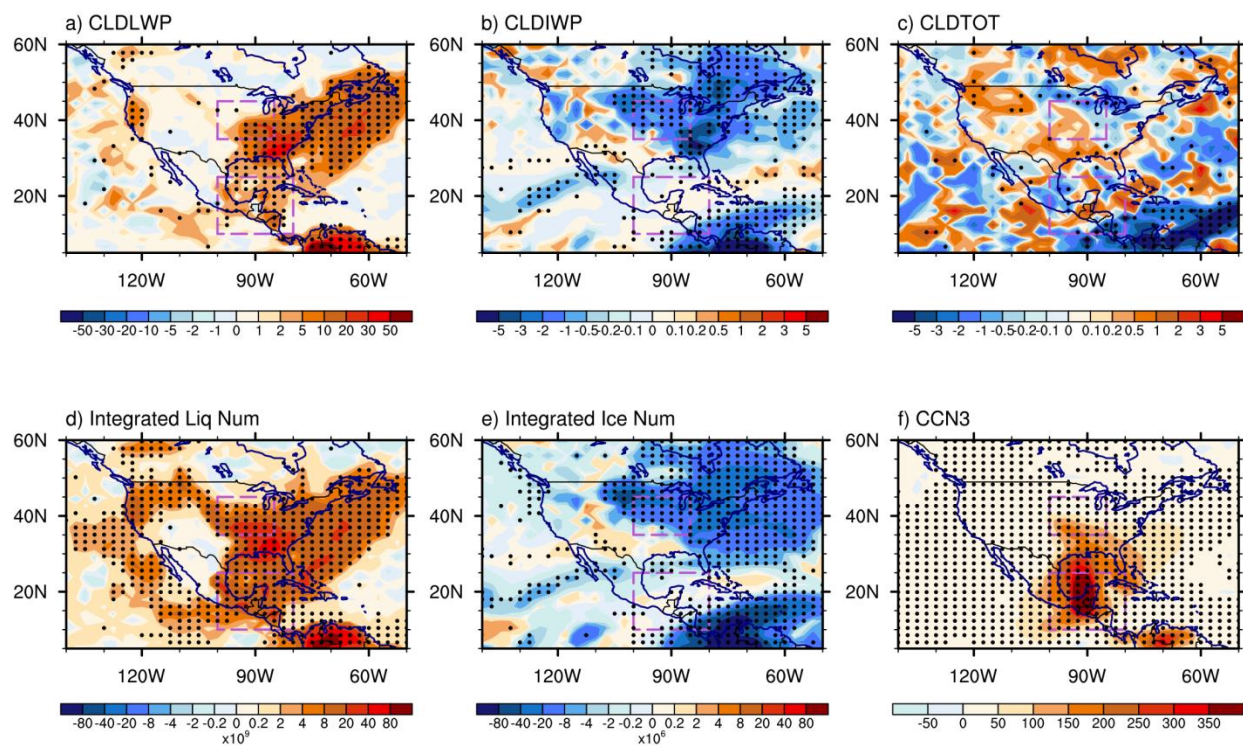


Figure 8. Difference of 10-day average (Apr.1-10) ensemble mean between simulations E\_NF and E\_QF: a) cloud liquid water path (  $\text{g m}^{-2}$  ), b) cloud ice water path (  $\text{g m}^{-2}$  ), c) total cloud fraction (%), d) column-integrated droplet number concentration (  $\text{m}^{-2}$  ), e) column-integrated ice number concentration (  $\text{m}^{-2}$  ), and f) cloud condensation nuclei at 0.1% supersaturation near 900 hPa. Dots denote regions where the difference is statistically significant at the 95% confidence level based on the KS test.

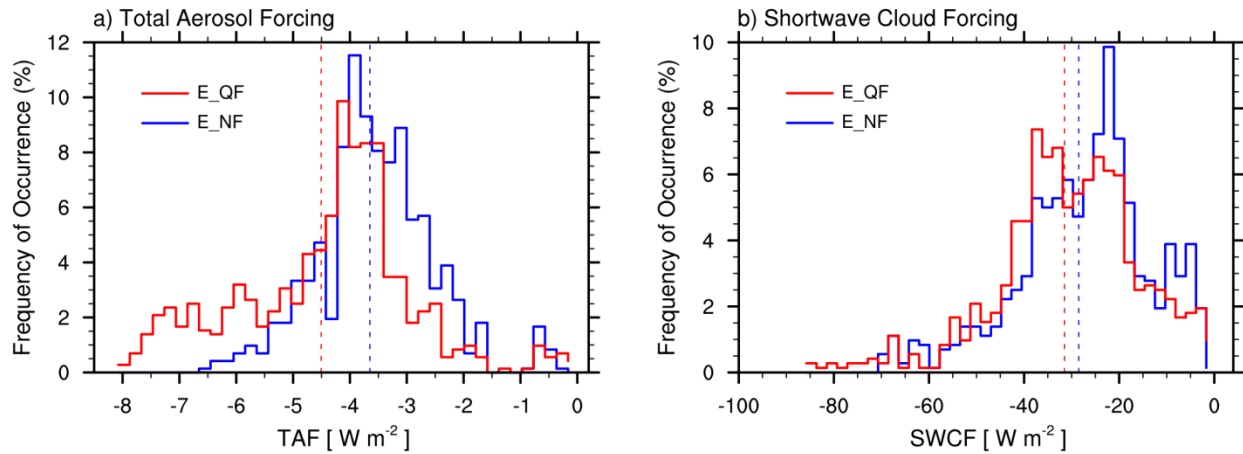


Figure 9. Probability distributions of 10-day average (Apr.1-10) a) total aerosol forcing and b) cloud forcing over Southern Mexico in simulations E\_NF and E\_QF sampled from grid values of ensemble members (72x10 for each case). Dashed lines indicate the mean of the distribution.

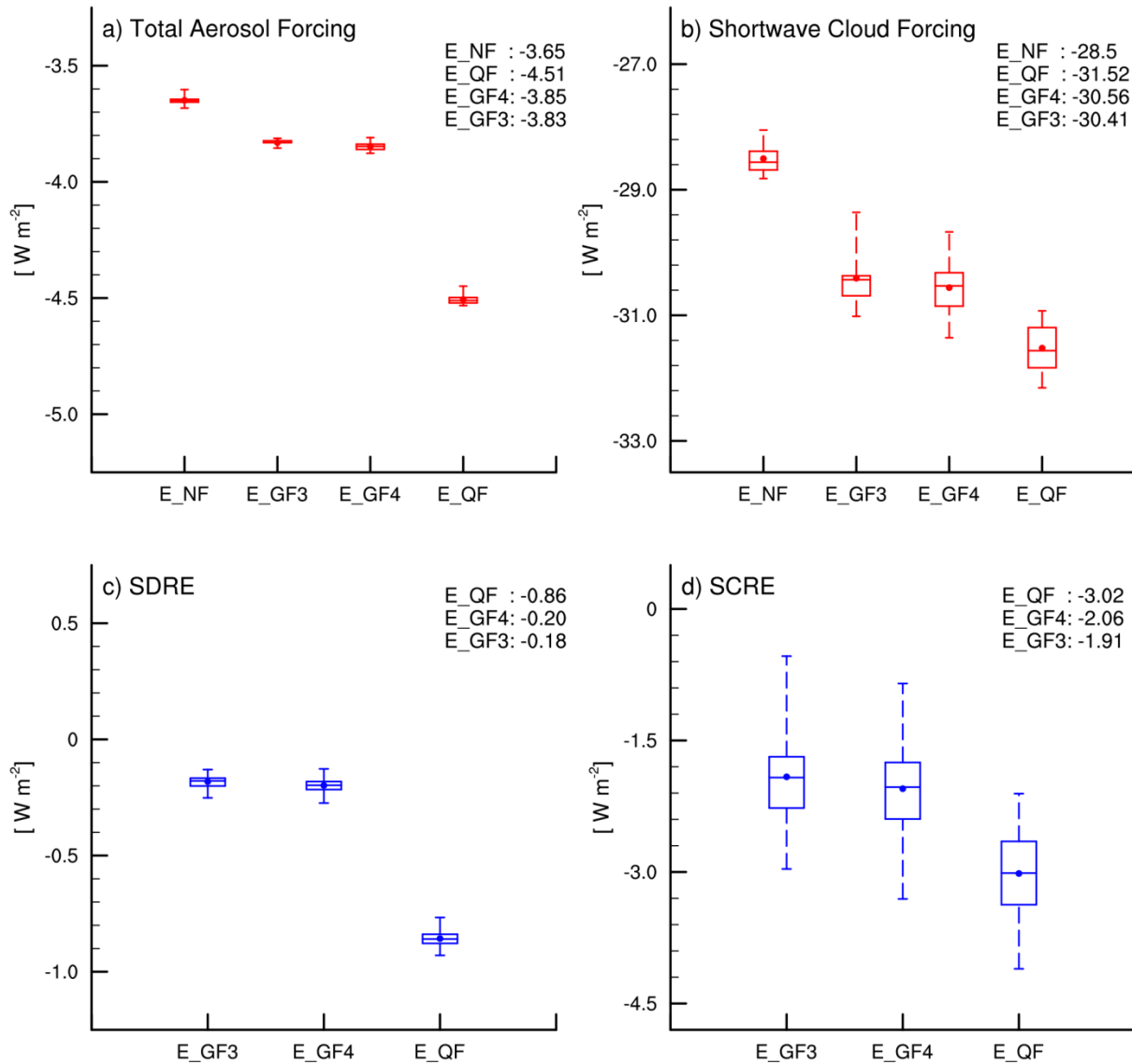


Figure 10. 10-day average (Apr. 1-10) regional mean a) total aerosol direct forcing, b) total shortwave cloud forcing and fire aerosol, c) SDRE, and d) SCRE in Southern Mexico in group B simulations. Box denotes the 25<sup>th</sup> and 75<sup>th</sup> percentiles. Bars outside the box indicate minimum and maximum. Bar within the box denotes the 50<sup>th</sup> percentile. Total aerosol and cloud forcing are sampled from different ensemble members (10 for each case). Fire aerosol SDRE and SCRF are sampled by calculating the difference between members in simulations E\_QF (E\_GF3/E\_GF4) and E\_NF (10x10 for each case).



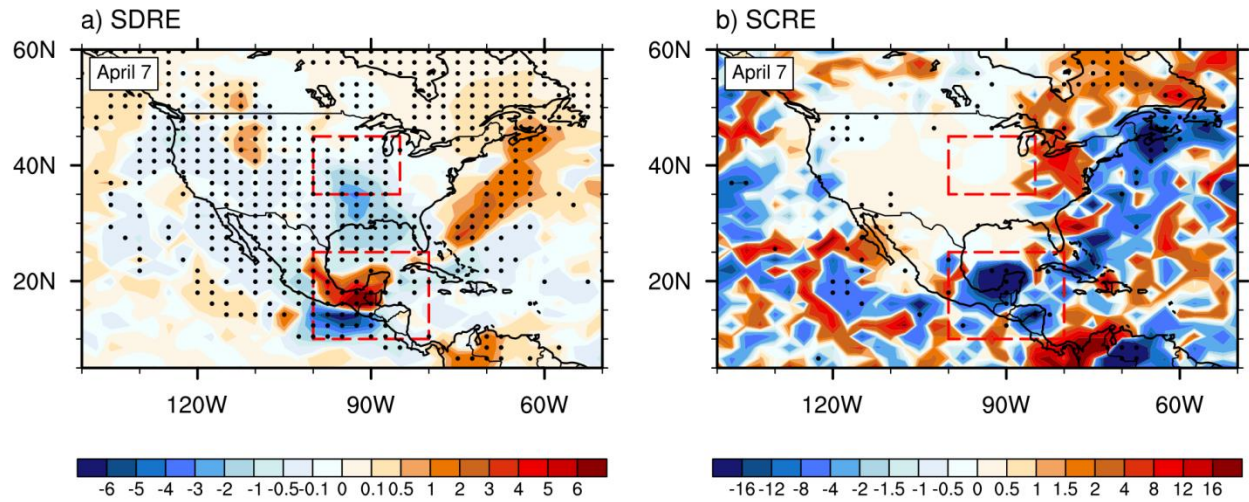


Figure 11. Spatial distributions of ensemble mean fire aerosol a) SDRE and b) SCRE ( $W m^{-2}$ ) on April 7 in the E\_QF simulation. Dots denote grids where fire aerosol effect is statistically significant at the 95% confidence level based on the KS test.

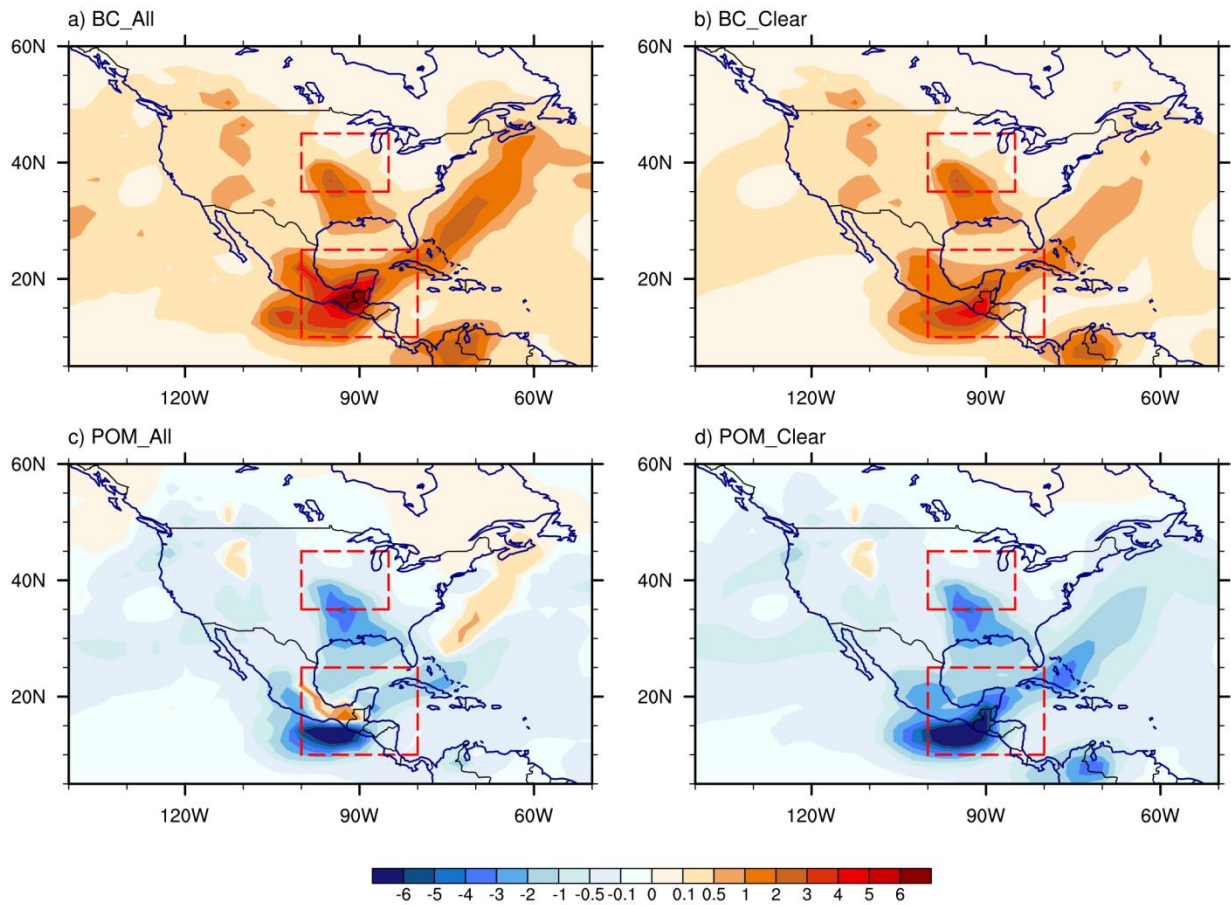


Figure 12. Spatial distributions of fire BC SDRE and fire POM SDRE (  $W m^{-2}$  ) on all-sky and clear-sky conditions on April 7 in the E\_QF simulation.

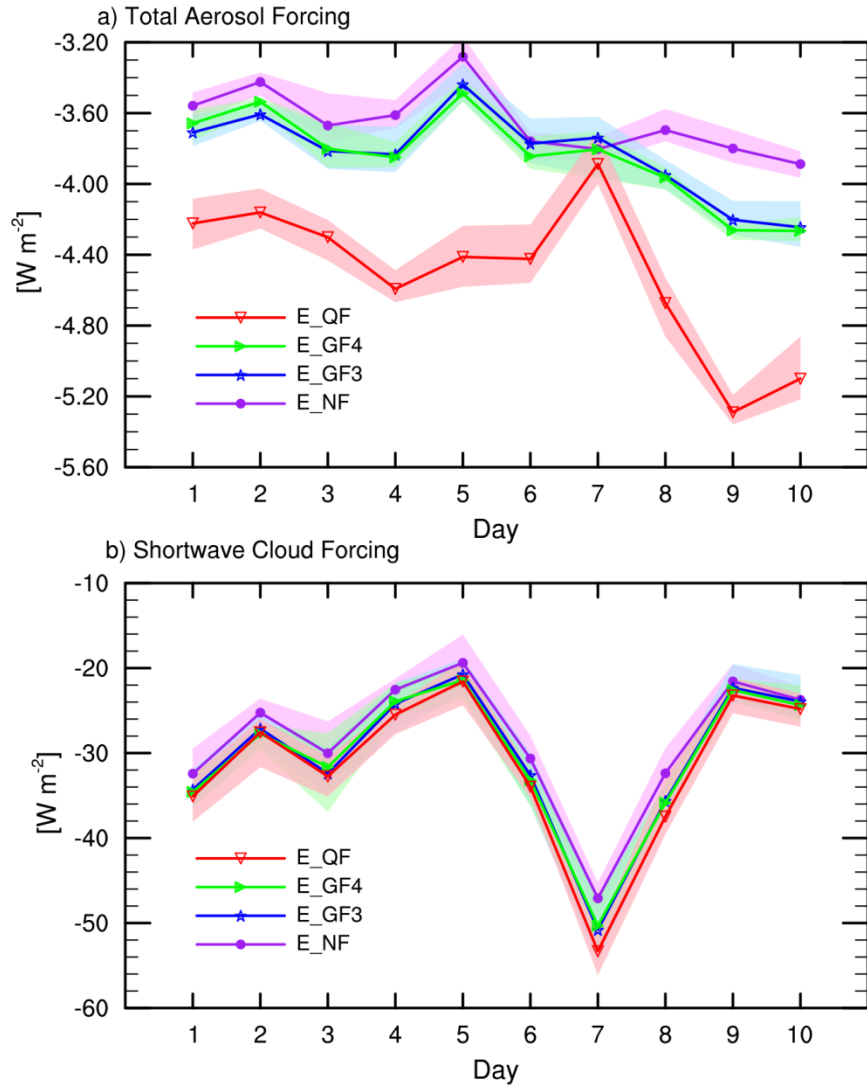


Figure 13. Time series of daily regional mean total a) aerosol forcing and b) cloud forcing in Southern Mexico during Apr.1-10, 2009 in group B simulations. Individual lines indicate ensemble mean values. Shaded areas illustrate the ensemble spread (from minimum to maximum).



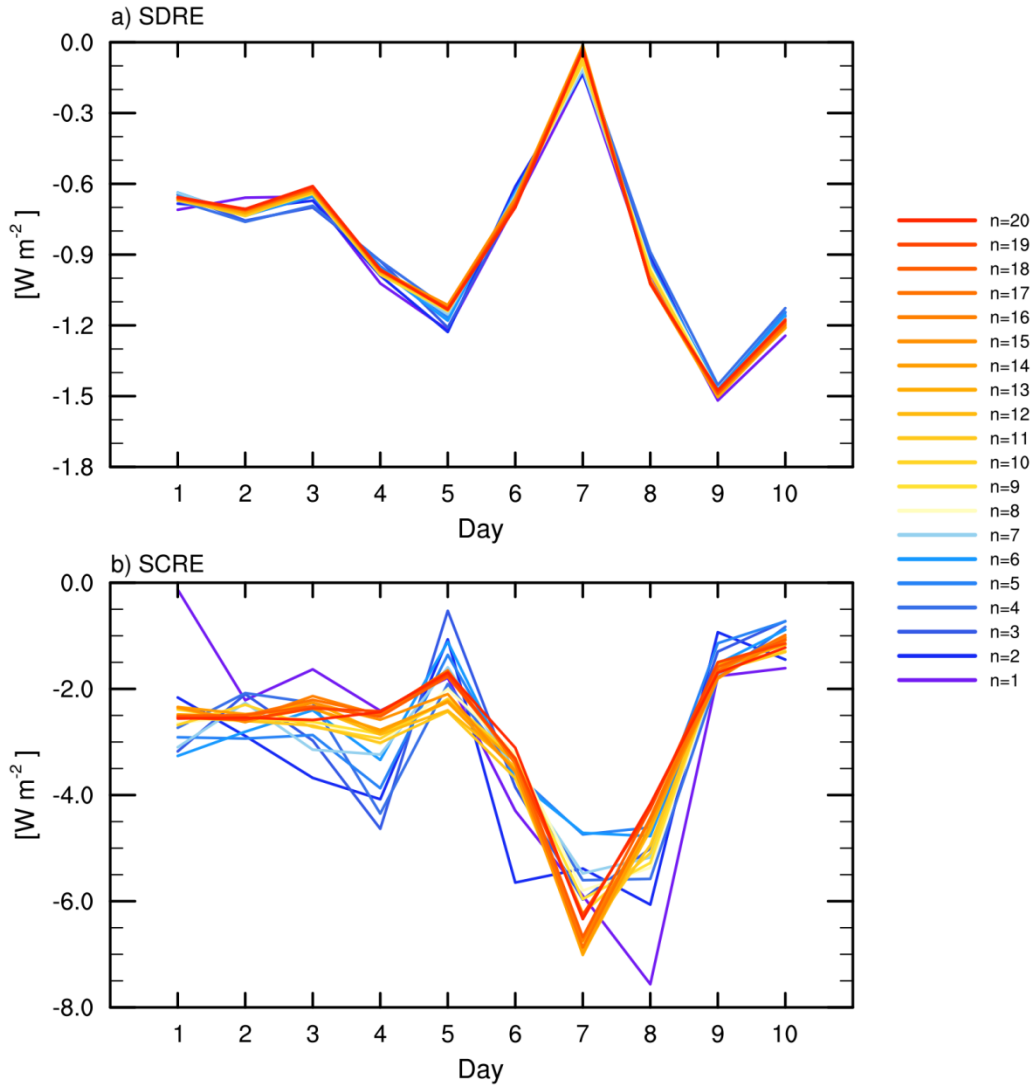


Figure 14. Time series of daily ensemble mean fire aerosol a) SDRE and b) SCRE averaged over Southern Mexico during Apr. 1-10, 2009 in QFED forced ensemble simulations with varying the total number of member numbers (n=1-20).

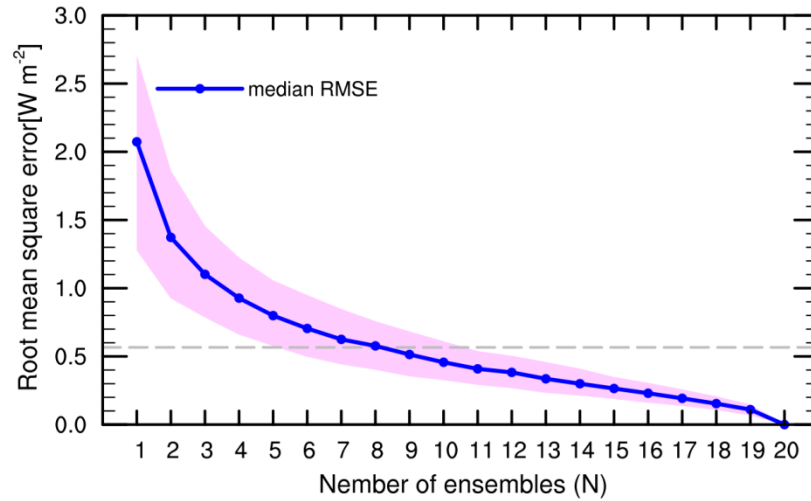


Figure 15 Root mean square errors (RMSE) of the ensemble mean of the regional mean fire aerosol SCRE during April 1-10 over Southern Mexico in simulations with different total number of ensemble members (N). The blue line represents the median RMSE of the 1000 groups (each group has N members/simulations). The grey line represents the threshold RMSE. Shaded area denotes the range between the 10<sup>th</sup> and 90<sup>th</sup> percentiles.

## Supplemental Materials

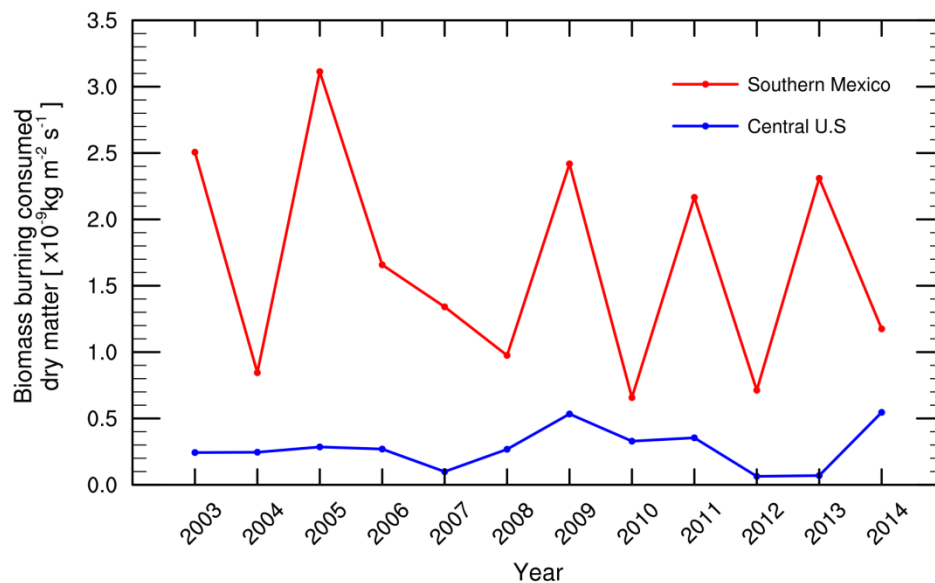


Figure S1. Time series of regional mean biomass burning consumed dry matter during April in central U.S (blue) and Mexico (red) from GFED v4.1.

Table S1 Regional mean emissions of fire aerosols in April, 2009 from three emission inventories (Unit:  $\times 10^{-12}$  kg m<sup>-2</sup>s<sup>-1</sup>). Numbers in the parentheses show results averaged in April 1-10.

	BC		OC		SO <sub>2</sub>	
	Central U.S.	Southern Mexico	Central U.S.	Southern Mexico	Central U.S.	Southern Mexico
GFED v3.1	0.25(0.38)	0.69(0.82)	1.82(3.58)	5.60(6.77)	1.35(2.01)	3.69(4.35)
GFED v4.1s	0.23(0.34)	1.17(1.44)	1.75(3.24)	8.80(10.76)	1.21(1.81)	6.25(7.69)
QFED v2.4	2.63(3.29)	3.87(3.87)	23.54(32.25)	36.81(36.58)	14.04(17.59)	20.62(20.65)

Table S2 Regional mean total AOD, fire AOD (difference in total AOD between simulations with and without fire) and the contributions of fire AOD (fire AOD divided by total AOD in the S\_NF simulation)during April, 2009 in group A simulations.

	Central U.S.			Southern Mexico		
	Total AOD	Fire AOD	Percentage	Total AOD	Fire AOD	Percentage
S_NF	0.066			0.130		
S_GF3	0.068	0.002	3.42%	0.141	0.011	8.10%
S_GF4	0.070	0.004	5.63%	0.145	0.015	11.20%
S_QF	0.099	0.033	49.33%	0.194	0.064	48.84%

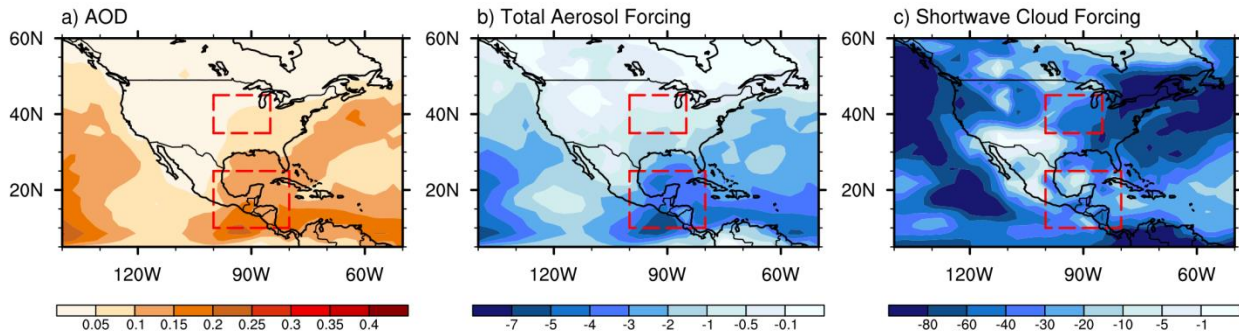


Figure S2. Spatial distributions of 10-day average (Apr. 1-10) ensemble mean a) AOD, b) total aerosol forcing and c) total shortwave cloud forcing(  $W m^{-2}$  ) in the simulation without fire emissions (E\_NF).

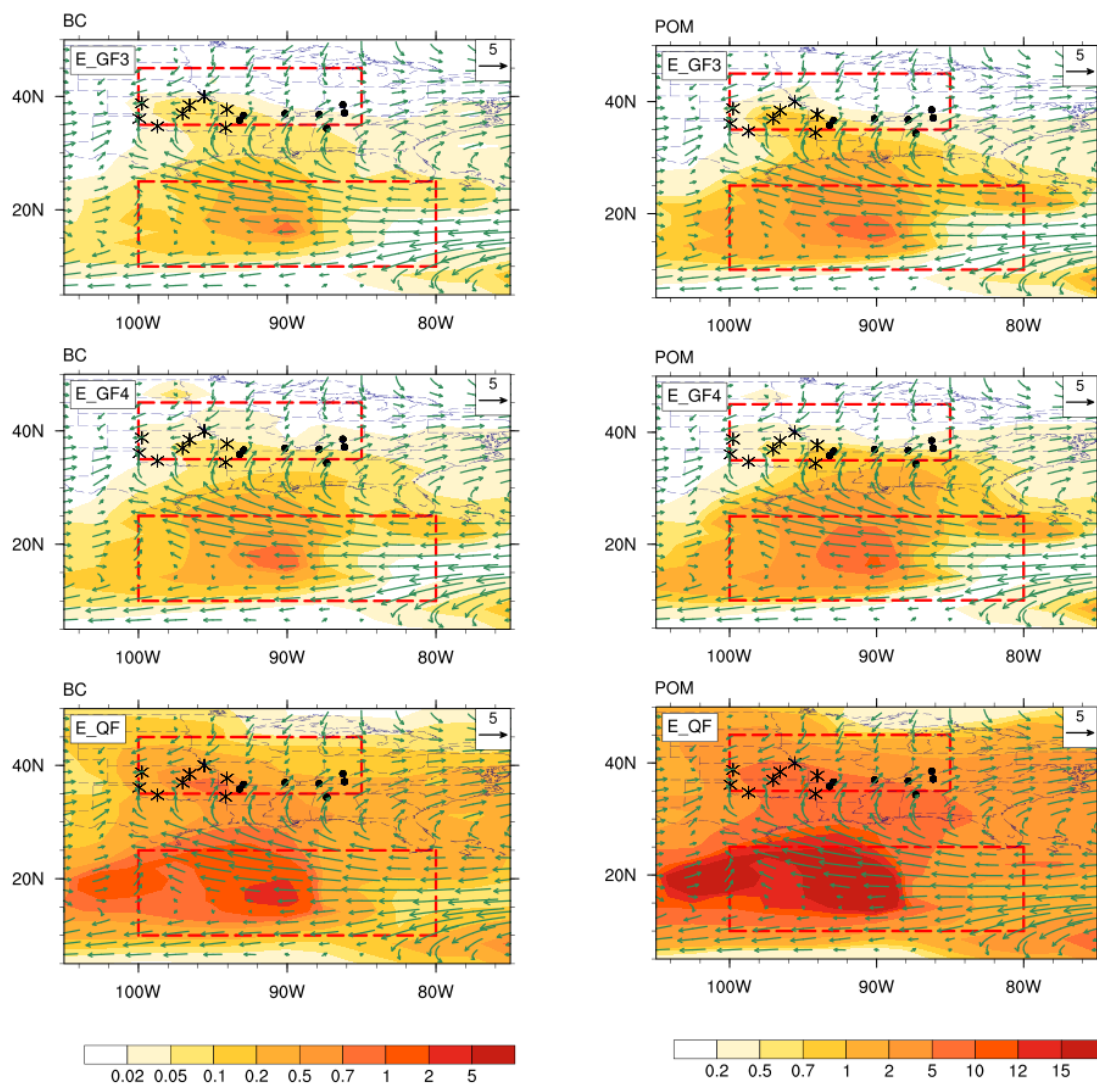


Figure S3. Spatial distributions of April mean fire BC and fire POM burden (shaded) on IMPROVE observation days in group B simulations (E\_GF3/E\_GF4/E\_QF – E\_NF). Vectors denote horizontal winds near 850hPa in group B fire simulations (E\_GF3/E\_GF4/E\_NF). IMPROVE data sites are marked with asterisks for sites near the source region and with dots for sites in the downwind region.

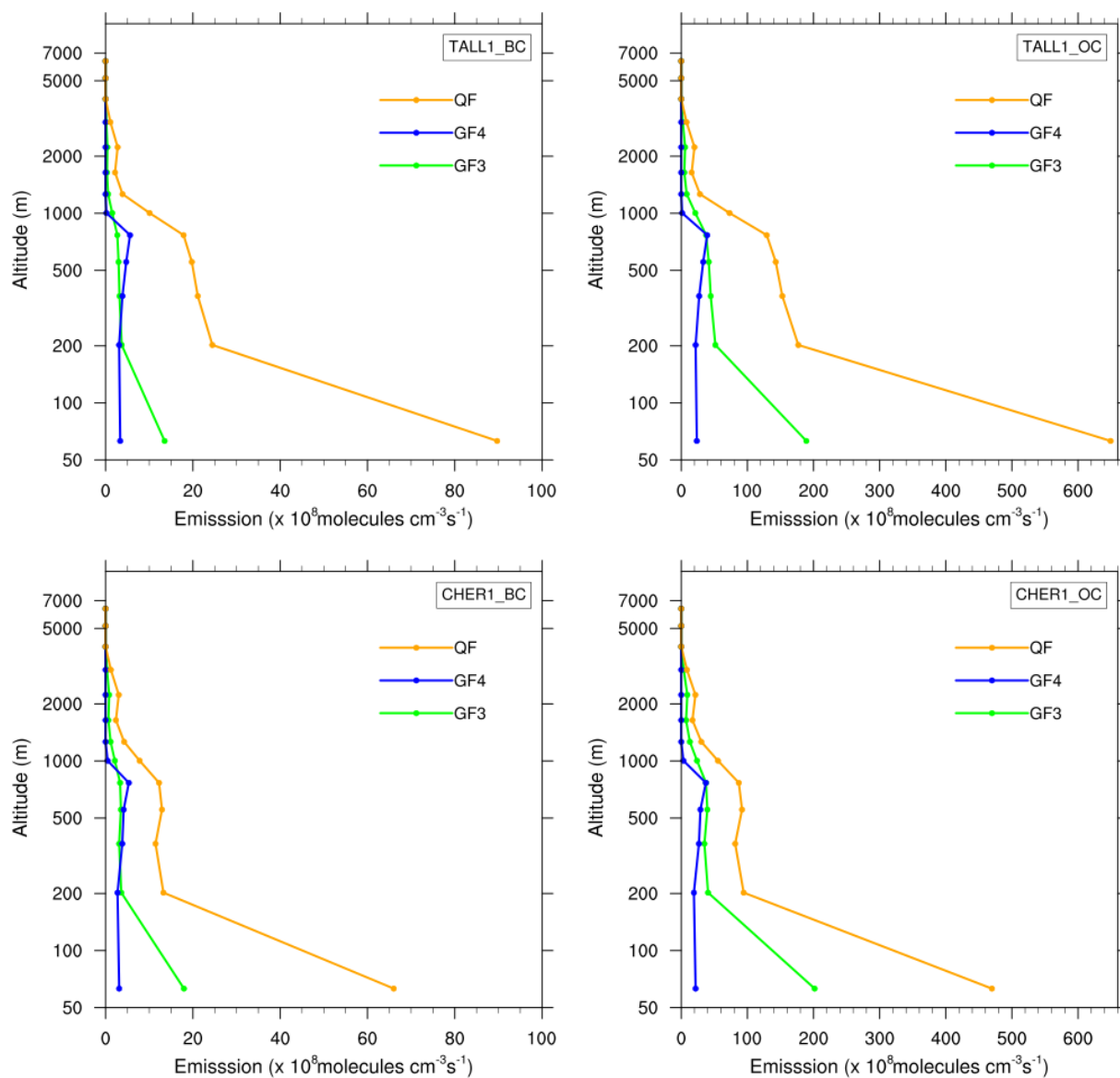


Figure S4. Vertical profiles of fire emissions of BC and OC used in simulations at sites TALL1 (38.43°N, 96.56°W) and CHER1 (38.77°N, 99.76°W).

Table S3 Regional mean total AOD, fire AOD (differences in AOD between simulations with and without fire) and radiative effects of fire aerosols during April 1-10, 2009 in group B simulations (Unit:  $W m^{-2}$ ). Total fire aerosol radiative effect is decomposed into shortwave direct radiative effect (SDRE), shortwave cloud radiative effect (SCRE), longwave cloud radiative effect (LCRE) and surface albedo effect (SAE).

	Total AOD	Fire AOD	SDRE	SCRE	LCRE	Total SAE
Central U.S.						
E_NF	0.047					
E_GF3	0.050	0.003	0.02	-0.86	0.04	0.02
E_GF4	0.050	0.003	-0.01	-0.39	0.002	-0.003
E_QF	0.08	0.033	-0.10	-0.56	-0.76	0.12
Southern Mexico						
E_NF	0.135					
E_GF3	0.149	0.014	-0.18	-1.91	-0.21	0.06
E_GF4	0.153	0.018	-0.20	-2.06	-0.23	0.11
E_QF	0.202	0.067	-0.86	-3.02	-0.47	0.14

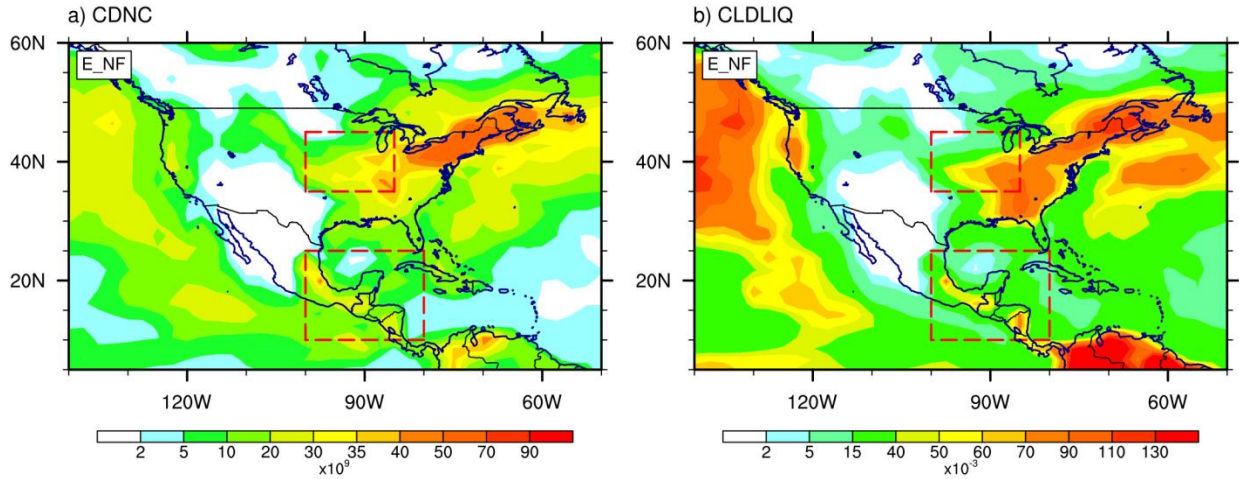


Figure S5. Spatial distributions of 10-day average (Apr. 1-10) ensemble mean a) column-integrated droplet number concentrations ( $\text{m}^{-2}$ ) and b) liquid water path ( $\text{g m}^{-2}$ ) in the E\_NF simulations.

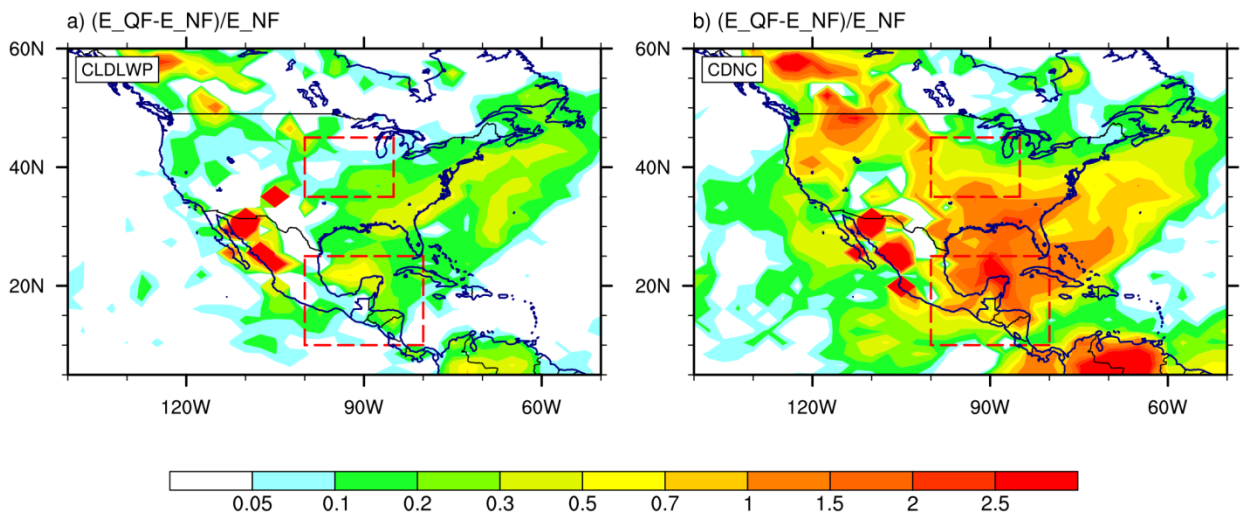


Figure S6. Relative changes of 10-day average ensemble mean cloud properties between the E\_NF and E\_QF simulations. a) cloud liquid water path, b) column-integrated droplet number concentration



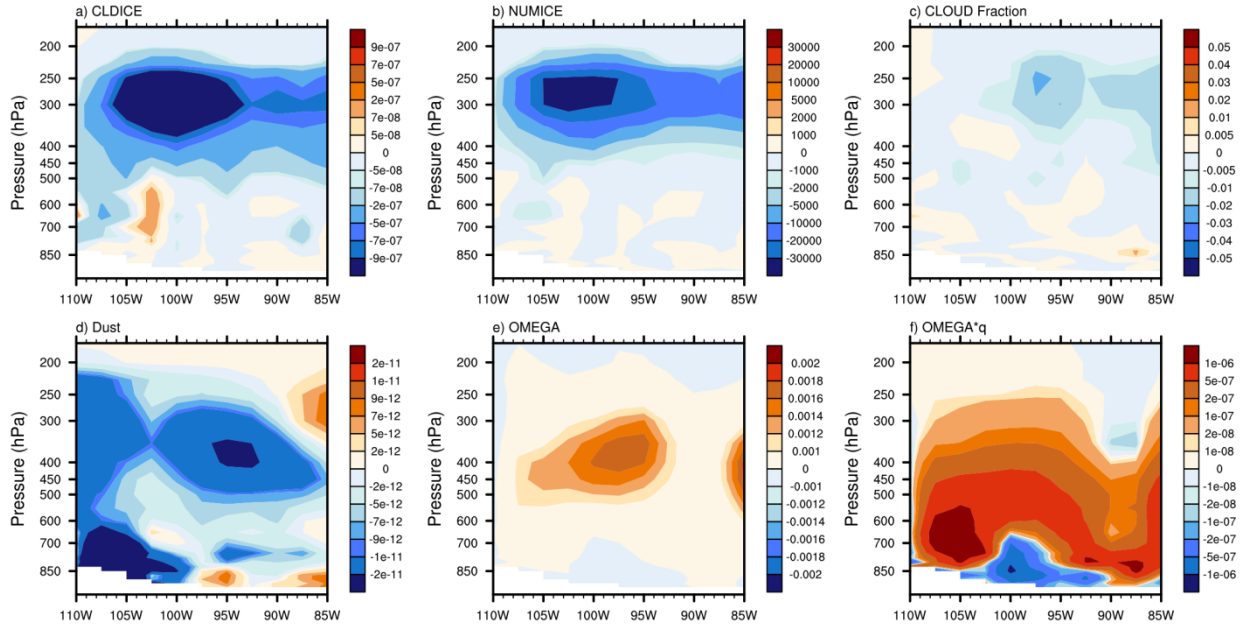


Figure S7. Pressure and longitude distribution of meridional mean ( $40\text{-}45^\circ\text{N}$ ) difference of 10-day average (April 1 -10) ensemble mean between simulation E\_NF and E\_QF: a) cloud ice amount ( $\text{kg} \cdot \text{kg}^{-1}$ ) b) cloud ice number concentration ( $\text{kg}^{-1}$ ) c) cloud fraction (1) d) Coarse mode dust concentration ( $\text{kg} \cdot \text{kg}^{-1}$ ) e) vertical velocity ( $\text{Pa} \cdot \text{s}^{-1}$ ) f) vertical moisture transport ( $\text{kg} \cdot \text{kg}^{-1} \cdot \text{Pa} \cdot \text{s}^{-1}$ )

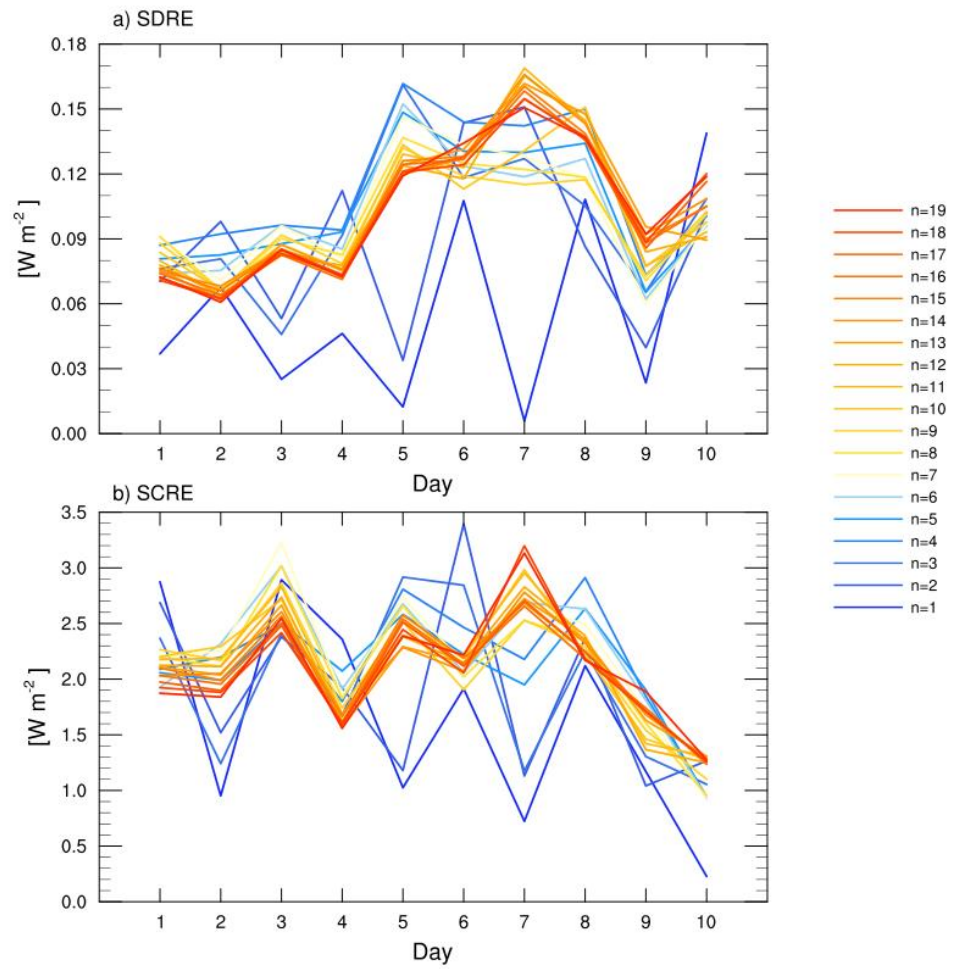


Figure S8. Time series of ensemble spread of daily regional mean fire aerosol a) SDRE and b) SCRE in Southern Mexico during Apr. 1-10, 2009 in QFED forced ensemble simulations with varying the total number of ensemble member (n=1-20).